BNL-99432-2013-TECH
C-A/AP/282;BNL-99432-2013-IR

Study of Orbits Produced by Individual Booster Extraction Bump Windings for the NASA Space Radiation Laboratory

L. Hammons

July 2007

Collider Accelerator Department
Brookhaven National Laboratory

U.S. Department of Energy
USDOE Office of Science (SC)

DISCLAIMER

C-A/AP/#282
July 2007

Study of Orbits Produced by Individual Booster Extraction Bump Windings for the NASA Space Radiation Laboratory

L. Hammons, L. Ahrens, K. Brown

Collider-Accelerator Department
Brookhaven National Laboratory
Upton, NY 11973

Study of Orbits Produced by Individual Booster Extraction Bump Windings for the NASA Space Radiation Laboratory

L. Hammons, L. Ahrens, K. Brown

Abstract

Orbit distortions caused by excitation of the Booster extraction windings for the NASA Space Radiation Laboratory (NSRL) transfer line were studied. Five windings form the extraction equipment under study, located at the C7, D1, D4, D7, and E1 Booster main magnet dipoles. Current was applied to each winding individually to study the effect on the orbit. The results of this effort are essential for designing a Booster extraction control system.

Beam position monitors were used to measure the orbit around the ring, and this data, along with MAD model data, was used to create a fit of the orbit to the model using the winding magnetic strength, the betatron tune, and the momentum spread as free parameters. The results of the fit were then compared to predicted results for each of the windings.

The study found consistent values for the tune when current was applied to each of the windings, and the experimental value of the tune differed from the set-point value by about 1%. In addition, the study also showed a very small momentum offset on the order of 10^{-5}. The magnitude of this offset was somewhat larger for the D4 and D7 windings.

The study also found a discrepancy between the predicted winding kicks and the observed kicks for each of the extraction windings of about 10% on the average. The cause of the difference is unclear, but may be caused either by a misunderstanding of the true field of the main magnet, the transfer function of the main magnet, or a combination of these factors. Further study of the transfer functions of the windings at various main magnet currents is required to pin down the source of the discrepancies.

Introduction

Booster slow extraction into the NSRL transfer line relies on three principal components: the resonant extraction sextupoles, two extraction septa located at D3 and D6 in the Booster, and a set of correction coils wound about each of five of the Booster main dipole magnets located at the C7, D1, D4, D7, and E1 positions. The windings are used to control the beam trajectory at the extraction septa, providing the potential for adjusting the position and angle of the beam at each of the septa. The relative locations of the septa and the windings are shown in figure 1.

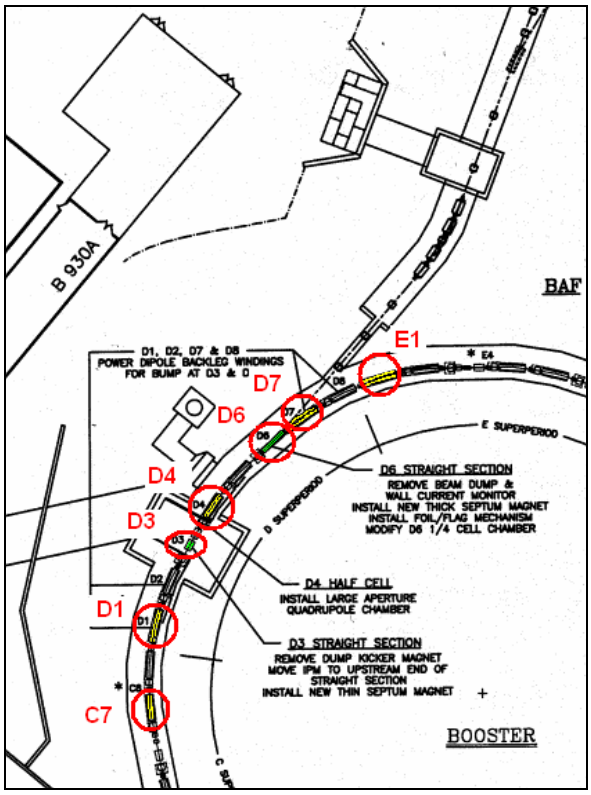

Figure 1 - Locations of correction windings and extraction septa.

The windings themselves consist of two turns around each dipole magnet and are powered individually by each of five power supplies. This provides a correction field to the main dipole magnet that is 1/8 as strong as the field produced by current in the main dipole winding for a given current (i.e. the dipole magnet consists of 16 turns). In addition, the dipole magnets are characterized by saturation effects particularly at currents above ~3000 A. The transfer function is plotted in figure 2, derived from the measurements of R. Thern [1]. The saturation of the main magnet dipole must, of course, be taken into account when calculating the change in field in the dipole magnets as a result of the main windings and the correction windings.

During the extraction process, the windings are individually powered with various currents so that the trajectory of the accelerated beam in the Booster is altered to provide optimum extraction efficiency. This study aims to collect orbit data for each of the windings at various currents in order to determine the transfer function for each winding.

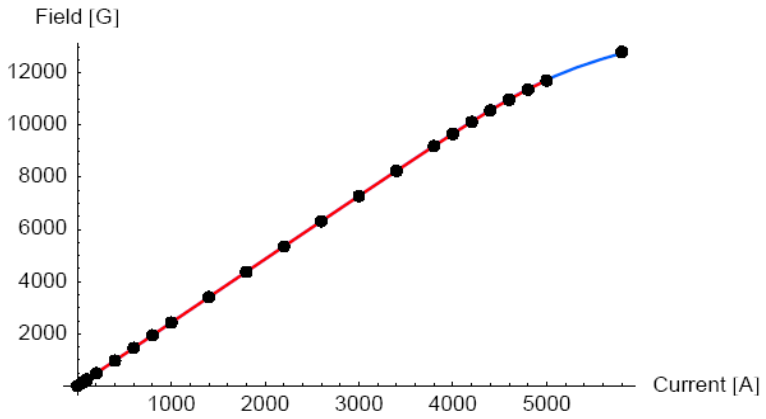

Figure 2 – Field curve for the Booster main magnet dipoles. The red curve is an interpolation function created using *Mathematica*. The blue curve is a fitting function generated by K. Brown (see (3) below). The interpolation function (4) is not properly defined beyond 5000 A, while the fitting function extends to the limit of known magnet data at 5800 A. Both the interpolation and the fitting function sit on top of each other up until 5000 A.

Theory

Orbit Bumps in the Booster

A deformation in the equilibrium orbit of an accelerator may be created with appropriate steering magnets or kickers. For the purpose of extracting beam to the NSRL transfer line, the deformation is realized through the use of additional coils wrapped around the main bending magnets as described above. The transverse position of the beam is described by:

$$x(s) = \frac{\theta_k \sqrt{\beta(s)\beta_k}}{2\sin\pi\upsilon} \cos(\left|\phi(s) - \phi_k\right| - \pi\upsilon) + D(s)\frac{dp}{p} \qquad (1)$$

where $\beta(s)$, $\phi(s)$, and $D(s)$ are the beta function, phase advance, and dispersion values at some point s around the ring; β_k and ϕ_k are the beta function and phase advance values at the point of the kicker or steering magnet; θ_k is angle imparted by the bump magnet, υ is the betatron tune of the machine, and dp/p is the momentum offset of the beam. In this experiment, θ_k, υ, and dp/p are constants of (1), determined using a least-squares fitting procedure to the data recorded by each of the available* beam position monitors in the Booster.

* Not all the Booster BPMs were available for measurement. The following BPMs were used: A4, A6, B4, B6, B8, C2, C6, C8, D2, D8, E2, E4, E6, F2, F4, and F8.

Predicted Kicks of the Correction Windings

After the values of θ_k, υ, and dp/p were determined using the fitting procedure, they were compared to the expected values for the experiment based on the currents flowing in the correction coils, the tune setpoint controlled by the *Optics-Control* application, and the expected momentum shift in the Booster for the bumps, which was assumed to be minimal.

The experimental and predicted kicks were of particular interest since these will be used ultimately to determine the transfer functions of each of the correction windings and establish a control system that will allow for precise control of the angle and position at both of the extraction septa.

The predicted kick was calculated by computing the magnetic field in the Booster dipole around which the correction coil is wound, taking into account the current in the main dipole as well as the current flowing in the coil. Each pole of a Booster main dipole is comprised of eight turns for a total of sixteen turns. The correction winding consists of two turns about a single pole in the main magnet. Thus, for the purpose of calculating the magnetic field, the total current flowing in the combined coil-main dipole magnet is given by:

$$I_{Total} = I_{Main} + \frac{2}{16} I_{Winding} \tag{2}$$

K. Brown [2] has constructed a polynomial description of the Booster main magnet field saturation curve shown in Figure 2 of the following form:

$$\begin{aligned} B(I) = {} & 9.122\times10^{-4} + 2.371\times10^{-4} I + 1.717\times10^{-8} I^2 - 2.412\times10^{-11} I^3 + 1.836\times10^{-14} I^4 \\ & -7.880\times10^{-18} I^5 + 1.891\times10^{-21} I^6 - 2.351\times10^{-25} I^7 + 1.163\times10^{-29} I^8 \end{aligned} \tag{3}$$

for use in the MAD model where I is the I_{Total} of (2).

Experiment

The Booster was set up to accelerate Fe^{+20} ions to 1 GeV nominal extraction energy over a magnet cycle of approximately 2000 ms in length. Acceleration required approximately 700 ms, and the full-energy, flattop field was maintained for approximately 650 ms, during which time, extraction into the NSRL line nominally would be expected. The main magnet field was set to 1.16 T at full field using the *BoosterMainMagnet* application, corresponding to a current set-

point of 4934.19 A at 960 ms after the beginning of the acceleration cycle (T0), the period during which orbit measurements were conducted. This, according to power supply personnel corresponds to an actual current of 4844.36 A due to a 2% discrepancy between the reference setting and current output of the main magnet power supply [3]. According to C. Gardner [4], this, in turn, corresponds to an actual magnetic field of 1.14 T for the Booster main dipoles. Extraction to the NSRL target was verified before the study conditions were established.

For the study, the RF gap voltage was maintained throughout the flattop to assure bunched beam for measurement by the beam position monitoring system in contrast to normal extraction where the RF is turned off just before beam is extracted. Furthermore, the Booster sextupoles were not used to excite resonant extraction, but rather were employed as a part of the chromaticity correction string, assuring that no extraction from the Booster would occur.

In addition, the following conditions prevailed throughout the study:

- Orbit measurements using the BPMs were conducted at 960 ms after the beginning of the acceleration cycle, well within the flattop regime of the main magnet and within the period during which the correction windings were powered.
- Beam was nominally centered in the machine during the flattop, and frequency measurements were conducted to verify the position. These measurements resulted in a beam revolution frequency of 3.90 MHz. Assuming a nominal Booster radius, this yielded a beam kinetic energy of 1.00×10^3 MeV.
- The Booster tune was set to 4.325 using the *OpticsControl* application.
- Beam was observed to survive with minimal losses in the Booster across the flattop.

Baseline orbit data from the BPM system was obtained during the flattop at 960 ms without applying current to any of the correction windings. Then, each of the windings (C7, D1, D4, D7, and E1) individually was powered to various currents within the range of the power supplies (±600 A) during the flattop, between 800 ms and 1200 ms after T0. The power supplies are calibrated to within ±2% of the requested setpoint [3]. The resulting perturbed orbits at each of the BPMs were recorded, taking the difference between the baseline data and the data collected while current flowed in the winding. In general, several meas-

urements were obtained at each winding current although in some cases, the data was lost because it had not been saved before the next acquisition.

BPM measurements were obtained using two methods: In the first, a data acquisition was triggered on ten Booster cycles using a gate width of 200 μs, each at the same time, and the results averaged. In the second method, ten acquisitions were obtained on the same Booster cycle, and the results averaged. The first method was used predominantly near the beginning of the study, and, to save time, the second method was employed near the midpoint of the study. Toward the end of the study, the first method was once again used. While no significant differences in the apparent quality of the data or the range of reported statistical errors was observed between the two methods, it is acknowledged that the second method could be a potential source of systematic errors.

Separately, the optics parameters, including the phase advances, the values of the beta functions, and the dispersion values at each BPM were obtained from the MAD model for each current applied to the correction windings. The Booster BPM data and the MAD model data were then combined to produce a least-squares fit to the orbit data using (1). The experimental value of the angle imparted by the bump winding, the tune, and the momentum offset were all used as free parameters, and the values were obtained through the fit procedure. Finally, the values of the kick were compared to predicted values based on the values of current and field in the main magnet and the correction windings. The tune and momentum were also compared.

Analysis

Perturbed Orbit Fitting Data

Tables 1 - 5 summarize the results of the fit procedure for each of the windings. Plots for each fit are included in figures 14 - 53. The quality of the fits, as suggested by the χ^2-statistics vary somewhat from measurement to measurement, and the normalized χ^2-statistic average is 0.80, suggesting reasonable agreement throughout the data sets between the experimental data and the model. Two important factors contribute to the individual variations in the fit calculations: the variation in the BPM measurements themselves and the accuracy and reliability of the model parameters generated by the MAD model.

The BPM system as a whole appears to be quite reliable, providing consistent measurements from trial to trial. BPM errors are also generally rather small, al-

though some of the BPMs, particularly C8 and F8, showed frequent malfunctions through the course of measurement. All of the BPM position data was averaged for each winding at each current, and some of the data points show correspondingly large errors. The error range does not change significantly between acquiring data on ten different acceleration cycles and acquiring ten samples on the same acceleration cycle.

MAD model parameters were generated by supplying the field errors in each of the main dipole magnets caused by each winding based on the current in the winding. The model was then run and the β-function values, phase advances, and momentum offsets at each of the BPMs were generated. The details of calculating these field errors are discussed below. The accuracy of all of the model parameters depends upon the accuracy of the predicted field errors. These field errors, in turn, were calculated based on the transfer function data measured by Thern and a knowledge of the nominal field of the Booster main magnet dipoles.

It should be noted that power supply variations in the bump windings are expected to be a negligibly small effect in the study, and that regulation errors for the power supply are less than 1%.

Kick, Tune, and Momentum Results

Kick, tune and momentum offsets are all free parameters in the fit, and the experimental values are generated through the fitting procedure. The results show consistent behavior throughout each of the trials. Both kick and tune results are especially consistent among each of the trials. The fit yielded an average tune value of 4.363±0.005, differing from the setpoint value of 4.325 by ~1%. A plot showing all of the tunes from each trial is shown in figure 3. Average values for all kicks are summarized in table 6. Plots of the kicks for each of the winding currents are given in figures 5 - 8.

Momentum offsets are quite small, conforming to the expectation that the bump introduces a small path-length change in the orbit. Given that the RF remains on throughout the measurement and that the RF works to keep the frequency fixed, a small momentum offset is the result. The momentum shift for the D4 and D7 windings is slightly larger and more varied, but also quite small. However, the pattern of momentum shifts is inconsistent among the five windings. While all of the windings appear to show a systematic momentum offset of ~7×10^{-5}, the C7 and D1 windings show a relatively flat offset for both positive and negative winding currents, while the D4, D7, and, to a lesser degree, the E1 windings

show momentum shifts whose sign and magnitude vary with the winding current. This behavior is consistent with the expectation that the orbit bump either increases or decreases the momentum offset based on the direction of the orbit perturbation. However, the C7 and D1 windings show no such variation current. This behavior is unexplained.

A plot showing all of the momentum shifts is shown in figure 4 along with the predicted momentum shifts calculated from the MAD model. The calculations are based on the change in path length reported by the MAD model for each winding excitation. The change in path length is given by the following expression:

$$\Delta L = \oint \left(\rho + D(s) \frac{\Delta p}{p_0} \right) d\theta - \oint \rho \, d\theta \tag{4}$$

where ΔL is the change in path length, ρ is the radius of curvature, $D(s)$ is the dispersion function, Δp is the change in momentum, p_0 is the nominal momentum, and θ is the angle around the ring. Then, the fractional change in path length is given by:

$$\frac{\Delta L}{L} = \frac{\oint D(s)\, ds / \rho}{\oint ds} \frac{\Delta p}{p} = \left\langle \frac{D}{\rho} \right\rangle \frac{\Delta p}{p_0} \tag{5}$$

and the fractional momentum shift is:

$$\frac{\Delta L}{L} \left\langle \frac{\rho}{D} \right\rangle = \frac{\Delta p}{p_0}. \tag{6}$$

The r.m.s. value of the dispersion function ~1.99 m, and the nominal radius of curvature is 13.866 m. The circumference of the ring (L) is 201.776 m, while the path length change ranges from 3.5 mm to -3.0 mm for the largest-magnitude winding currents. Notice in figure 4 that the model shifts show consistent behavior throughout all of the windings and a maximum shift of ~1×10^{-5}. This is the same order as the momentum shifts determined by the fit procedure.

In order to investigate the nature of the momentum shift more thoroughly, we also attempted to compare the kicks and tunes with dp/p fixed at zero with the values determined from the fit for C7, which shows the least variation in momen-

tum spread with kick strength and D4, which shows the greatest variation, thereby gauging the contribution of the momentum offset to the transverse position. The results appear in figures 5 – 8. Both the kick and tune values for each winding in each case are practically indistinguishable from each other, and suggest that the impact on transverse position, kick strength, and tune is minimal. Evidently, whatever the momentum shift, it is a rather small effect.

Comparison of Experimental and Predicted Kicks from Bump Windings

After the closed orbit distortions were obtained, a comparison of the experimental and predicted kicks for each winding was conducted. The predicted kicks were calculated based on the transfer function data documented by Thern as noted above. Plots of the data appears in figures 9 - 13. To determine the total field in each dipole magnet associated with a winding, the total current in the dipole was calculated using equation (2), and a polynomial interpolation function of the data was created using *Mathematica.** This generated the following expression for field as a function of current:

$$\begin{aligned} B(I) = {} & 7.772 + 2.39400I + 3.10859\times10^{-5} I^{2} + 1.13323\times10^{-6} I^{3} - \\ & 1.09351\times10^{-8} I^{4} + 5.21323\times10^{-11} I^{5} - 1.53052\times10^{-13} I^{6} + \\ & 3.02965\times10^{-16} I^{7} - 4.27034\times10^{-19} I^{8} + 4.44496\times10^{-22} I^{9} - \\ & 3.50344\times10^{-25} I^{10} + 2.13690\times10^{-28} I^{11} - 1.00536\times10^{-31} I^{12} + \\ & 3.72063\times10^{-35} I^{13} - 1.07850\times10^{-38} I^{14} + 2.43668\times10^{-42} I^{15} - \\ & 4.24213\times10^{-46} I^{16} + 5.57675\times10^{-50} I^{17} - 5.35105\times10^{-54} I^{18} + \\ & 3.53456\times10^{-58} I^{19} - 1.4362\times10^{-62} I^{20} + 2.70502\times10^{-67} I^{21} \end{aligned} \qquad (4)$$

The plots show that the predicted kick is consistently larger in magnitude than the experimentally determined value for all of the winding currents. The cause of this deviation is unclear, but may arise from several sources, the most important of which are a deviation in the main magnet field, a deviation in the winding field, an incorrect understanding of the transfer function for the main magnet, or some combination of these factors. The winding current was monitored during the study, and showed very little variation.

The main magnet field for the Booster is a more complicated factor in the analysis due to the saturation of the transfer function at the fields and currents required for extraction of 1 GeV iron. To understand the nature of the main mag-

* Wolfram Research, Inc.

net function, several attempts were made to carefully model the transfer function based on data obtained by Thern, and ultimately resulted in using a polynomial interpolation function implemented in *Mathematica* whose polynomial representation is given in equation (4). Calculation of the field is further complicated by the discrepancy between the main magnet current and field setpoints and the actual field generated for a given setpoint. Gardner regularly publishes a listing of the required setpoints, the resulting fields generated, and this listing was used as the basis for this study.

After comparison of the experimental and predicted kicks in the windings, a least-squares fit of the predicted kicks to experiment was employed using the main magnet current as a free parameter. This analysis showed that the best fit between prediction and experiment is obtained when the current is increased by approximately 2%. This, in turn, also changes the total field in the main magnet (main magnet field plus bump winding field) by 2%. This is equivalent to a change in the bump currents of 11%. Since this error well exceeds the known current error in the winding, it appears likely that our understanding of the main magnet current and field is incorrect.

Increasing the main magnet field has the effect of reducing the magnitude of all the predicted kicks, presumably moving the main magnet field along the saturation and changing the slopes of the predicted data points. It is difficult to distinguish, with such a limited set of data points, whether errors arise from an incorrect understanding of the field or an incorrect understanding of the saturation curve. Further study of the main magnet field and the relation of current setpoints to actual fields in the main magnet, particularly at the highest currents in the magnet is required in order to reconcile the results obtained in this study. In addition, it would be especially useful to collect further bump data using the method described in this study at various main magnet fields. This data would serve as a map of the saturation function and would allow confirmation of the data obtained by Thern as well as the saturation model expressed in (4).

Conclusions

Transfer functions for each of the NSRL extraction bump windings was obtained in this study. The fit results for the tune are consistent for each winding current and vary from the tune setpoint by 1%.

In addition, the momentum offset is very small, consistent with the expectation that the total path length change is very small. However, there is a somewhat

larger, albeit still quite small, momentum shift for the D4 and D7 windings. The pattern of these momentum offsets is somewhat inconsistent from winding to winding, and the cause of this inconsistency is unclear.

The fit results for the kicks also show consistent results for each of the windings. However, a comparison with expectations for the kick strengths shows a difference of 10%. The variation appears unlikely to arise from errors in the windings, but is more likely to arise from an incorrect understanding of the main magnet field or the saturation of the main magnet field at high current. Further study of the winding transfer functions is necessary at various main magnet currents is necessary to pin down the source of these deviations.

Table 1 - Fit Results for the C7 Winding

Current (A)	Trial	θ (rad)	Tune (υ)	dp / p	Norm. χ^2
-400	1	$-1.272 \pm 0.008\times10^{-3}$	4.363 ± 0.002	$5.9 \pm 1.3\times10^{-5}$	1.23
-400	2	$-1.288 \pm 0.009\times10^{-3}$	4.365 ± 0.003	$4.6 \pm 1.8\times10^{-5}$	1.12
-200	1	$-6.394 \pm 0.064\times10^{-4}$	4.362 ± 0.004	$6.3 \pm 1.2\times10^{-5}$	0.52
-200	2	$-6.390 \pm 0.090\times10^{-4}$	4.367 ± 0.005	$3.8 \pm 1.6\times10^{-5}$	0.37
200	1	$6.144 \pm 0.087\times10^{-4}$	4.359 ± 0.005	$6.0 \pm 1.6\times10^{-5}$	0.31
200	2	$6.086 \pm 0.078\times10^{-4}$	4.357 ± 0.005	$5.3 \pm 1.5\times10^{-5}$	0.80
400	1	$1.245 \pm 0.007\times10^{-3}$	4.356 ± 0.002	$3.9 \pm 1.3\times10^{-5}$	1.11
400	2	$1.253 \pm 0.008\times10^{-3}$	4.359 ± 0.003	$6.1 \pm 1.5\times10^{-5}$	1.01
550*	1	$1.715 \pm 0.007\times10^{-3}$	4.359 ± 0.002	$6.4 \pm 1.3\times10^{-5}$	2.03
550*	2	$1.711 \pm 0.009\times10^{-3}$	4.360 ± 0.002	$6.8 \pm 0.9\times10^{-5}$	1.61
				Avg. Norm. χ^2	0.84

*For this data set, current of 550A was also applied to show the response near the limit of the power supply. This data point does not appear in the other winding data sets.

Table 2 - Fit Results for the D1 Winding

Current (A)	Trial	θ (rad)	Tune (υ)	dp / p	Norm. χ^2
-400	1	$-1.252 \pm 0.008\times10^{-3}$	4.365 ± 0.002	$9.2 \pm 1.2\times10^{-5}$	1.35
-200	1	$-6.300 \pm 0.011\times10^{-4}$	4.363 ± 0.006	$5.8 \pm 1.9\times10^{-5}$	0.51
200	1	$6.188 \pm 0.131\times10^{-4}$	4.369 ± 0.006	$5.5 \pm 2.3\times10^{-5}$	0.40
200	2	$6.192 \pm 0.089\times10^{-4}$	4.369 ± 0.004	$8.0 \pm 1.5\times10^{-5}$	0.89
400	1	$1.242 \pm 0.001\times10^{-3}$	4.366 ± 0.002	$8.2 \pm 2.0\times10^{-5}$	0.97
400	2	$1.236 \pm 0.010\times10^{-3}$	4.361 ± 0.002	$3.4 \pm 1.6\times10^{-5}$	1.66
				Avg. Norm. χ^2	0.72

Table 3 - Fit Results for the D4 Winding

Current (A)	Trial	θ (rad)	Tune (υ)	dp / p	Norm. χ^2
-400	1	$-1.265 \pm 0.006\times10^{-3}$	4.364 ± 0.002	$-6.0 \pm 1.2\times10^{-5}$	1.40
-400	2	$-1.258 \pm 0.096\times10^{-3}$	4.362 ± 0.006	$-5.4 \pm 1.8\times10^{-5}$	0.71
-200	1	$-6.245 \pm 0.117\times10^{-4}$	4.362 ± 0.006	$0.1 \pm 2.2\times10^{-5}$	0.17
-200	2	$-6.144 \pm 0.081\times10^{-4}$	4.358 ± 0.002	$3.1 \pm 1.5\times10^{-5}$	0.93
200	1	$6.210 \pm 0.076\times10^{-4}$	4.365 ± 0.004	$1.1 \pm 0.1\times10^{-4}$	0.31
200	2	$6.380 \pm 0.090\times10^{-4}$	4.366 ± 0.004	$4.9 \pm 1.6\times10^{-5}$	0.74
400	1	$1.238 \pm 0.008\times10^{-3}$	4.366 ± 0.001	$2.1 \pm 0.1\times10^{-4}$	1.33
400	2	$1.266 \pm 0.008\times10^{-3}$	4.370 ± 0.002	$1.7 \pm 0.2\times10^{-4}$	2.22
				Avg. Norm. χ^2	0.78

Table 4 - Fit Results for D7 Winding

Current (A)	Trial	θ (rad)	Tune (υ)	dp / p	Norm. χ^2
-400	1	$-1.273 \pm 0.012\times10^{-3}$	4.367 ± 0.002	$-2.1 \pm 2.0\times10^{-5}$	0.95
-400	2	$-1.264 \pm 0.011\times10^{-3}$	4.364 ± 0.002	$1.1 \pm 1.6\times10^{-5}$	1.25
-200	1	$-6.291 \pm 0.113\times10^{-4}$	4.363 ± 0.004	$2.3 \pm 1.8\times10^{-5}$	0.42
-200	2	$-6.254 \pm 0.084\times10^{-4}$	4.360 ± 0.003	$0.1 \pm 1.2\times10^{-5}$	1.10
200	1	$6.102 \pm 0.112\times10^{-4}$	4.360 ± 0.004	$1.4 \pm 0.2\times10^{-4}$	0.32
200	2	$6.176 \pm 0.087\times10^{-4}$	4.369 ± 0.003	$9.3 \pm 1.2\times10^{-5}$	0.54
400	1	$1.244 \pm 0.009\times10^{-3}$	4.364 ± 0.002	$1.7 \pm 0.2\times10^{-4}$	1.42
400	2	$1.249 \pm 0.013\times10^{-3}$	4.364 ± 0.002	$1.7 \pm 0.2\times10^{-4}$	0.72
				Avg. Norm. χ^2	0.67

Table 5 - Fit Results for E1 Winding

Current (A)	Trial	θ (rad)	Tune (υ)	dp / p	Norm. χ^2
-400	1	$-1.276 \pm 0.008\times10^{-3}$	4.366 ± 0.002	$0.7 \pm 1.4\times10^{-5}$	0.92
-400	2	$-1.276 \pm 0.008\times10^{-3}$	4.366 ± 0.002	$0.6 \pm 1.5\times10^{-5}$	0.92
-200	1	$-6.387 \pm 0.064\times10^{-4}$	4.366 ± 0.003	$6.3 \pm 1.0\times10^{-5}$	1.64
-200	2	$-6.022 \pm 0.066\times10^{-4}$	4.355 ± 0.004	$7.0 \pm 1.2\times10^{-5}$	2.01
200	1	$6.222 \pm 0.077\times10^{-4}$	4.362 ± 0.004	$5.7 \pm 1.2\times10^{-5}$	0.41
200	2	$6.222 \pm 0.076\times10^{-4}$	4.362 ± 0.004	$5.7 \pm 1.2\times10^{-5}$	0.41
400	1	$1.257 \pm 0.007\times10^{-3}$	4.361 ± 0.002	$7.4 \pm 1.2\times10^{-5}$	1.01
400	2	$1.255 \pm 0.009\times10^{-3}$	4.360 ± 0.002	$9.9 \pm 1.6\times10^{-5}$	0.41
				Avg. Norm. χ^2	0.77

Table 6 - Averaged Fit Results for All Winding Currents

Current (A)	θ (rad)	Tune (υ)	dp / p
-400	$-1.270 \pm 0.009\times10^{-3}$	4.363 ± 0.003	$6.7 \pm 5.8\times10^{-5}$
-200	$-6.270 \pm 0.093\times10^{-4}$		
200	$6.192 \pm 0.081\times10^{-4}$		
400	$1.249 \pm 0.009\times10^{-3}$		

Table 7 – Average Experimental and Predicted Kick for C7 Winding

Winding Current (A)	Experimental Kick (rad)	Predicted Kick Before Fit (rad)	Predicted Kick After Fit (rad)	% Diff. Before Fit	% Diff. After Fit	Total Field (Main Magnet + Bump) Before Fit (T)	Total Field (Main Magnet + Bump) After Fit (T)
-400	$-1.281 \pm 0.009 \times 10^{-3}$	-1.410×10^{-3}	-1.334×10^{-3}	9.17	4.01	1.133	1.152
-200	$-6.31 \pm 0.08 \times 10^{-4}$	-6.94×10^{-4}	-6.605×10^{-4}	7.92	3.22	1.138	1.156
200	$6.11 \pm 0.08 \times 10^{-4}$	7.080×10^{-4}	6.406×10^{-4}	13.64	4.53	1.147	1.16
400	$1.252 \pm 0.008 \times 10^{-3}$	1.393×10^{-3}	1.250×10^{-3}	10.08	-0.24	1.151	1.16

Expected Main Magnet Current (A)	4836.43	Expected Main Magnet Field (T)	1.142	Norm. χ^2	298.62
Fitted Main Magnet Current (A)	4939.08	Fitted Main Magnet Field (T)	1.161	Norm. χ^2	18.95

Table 8 - Average Experimental and Predicted Kick for D1 Winding

Winding Current (A)	Experimental Kick (rad)	Predicted Kick Before Fit (rad)	Predicted Kick After Fit (rad)	% Diff. Before Fit	% Diff. After Fit	Total Field (Main Magnet + Bump) Before Fit (T)	Total Field (Main Magnet + Bump) After Fit (T)
-400	$-1.252 \pm 0.008 \times 10^{-3}$	-1.41×10^{-3}	-1.316×10^{-3}	10.56	5.04	1.133	1.154
-200	$-6.30 \pm 0.2 \times 10^{-4}$	-6.9×10^{-4}	-6.495×10^{-4}	11.88	2.99	1.138	1.159
200	$6.20 \pm 0.1 \times 10^{-4}$	7.1×10^{-4}	6.241×10^{-4}	9.92	0.82	1.147	1.167
400	$1.239 \pm 0.1 \times 10^{-3}$	1.39×10^{-3}	1.209×10^{-3}	10.06	-2.49	1.151	1.171

Expected Main Magnet Current (A)	4836.43	Expected Main Magnet Field (T)	1.143	Norm. χ^2	181.97
Fitted Main Magnet Current (A)	4952.56	Fitted Main Magnet Field (T)	1.163	Norm. χ^2	15.77

Table 9 – Average Experimental and Predicted Kick for D4 Winding

Winding Current (A)	Experimental Kick (rad)	Predicted Kick Before Fit (rad)	Predicted Kick After Fit (rad)	% Diff. Before Fit	% Diff. After Fit	Total Field (Main Magnet + Bump) Before Fit (T)	Total Field (Main Magnet + Bump) After Fit (T)
-400	$-1.261 \pm 0.008\times10^{-3}$	-1.410×10^{-3}	-1.358×10^{-3}	10.52	4.67	1.133	1.177
-200	$-6.19 \pm 0.10\times10^{-4}$	-6.94×10^{-4}	-6.698×10^{-4}	10.76	5.30	1.138	1.179
200	$6.29 \pm 0.08\times10^{-4}$	7.08×10^{-4}	6.879×10^{-4}	11.09	0.26	1.147	1.181
400	$1.252 \pm 0.008\times10^{-3}$	1.393×10^{-3}	1.361×10^{-3}	10.13	-2.11	1.151	1.179

Expected Main Magnet Current (A)	4836.43	Expected Main Magnet Field (T)	1.143	Norm. χ^2	245.83
Fitted Main Magnet Current (A)	4947.21	Fitted Main Magnet Field (T)	1.181	Norm. χ^2	27.18

Table 10 – Average Experimental and Predicted Kick for D7 Winding

Winding Current (A)	Experimental Kick (rad)	Predicted Kick Before Fit (rad)	Predicted Kick After Fit (rad)	% Diff. Before Fit	% Diff. After Fit	Total Field (Main Magnet + Bump) Before Fit (T)	Total Field (Main Magnet + Bump) After Fit (T)
-400	$-1.27 \pm 0.01\times10^{-3}$	-1.410×10^{-3}	-1.410E-03	10.04	3.81	1.133	1.154
-200	$-6.27 \pm 0.10\times10^{-4}$	-6.94×10^{-4}	-6.941E-04	10.77	3.71	1.138	1.158
200	$6.14 \pm 0.01\times10^{-4}$	7.08×10^{-4}	7.081E-04	12.15	2.18	1.147	1.167
400	$1.246 \pm 0.002\times10^{-3}$	1.393×10^{-3}	1.393E-03	10.47	-2.41	1.151	1.171

Expected Main Magnet Current (A)	4836.43	Expected Main Magnet Field (T)	1.143	Norm. χ^2	138.55
Fitted Main Magnet Current (A)	4950.18	Fitted Main Magnet Field (T)	1.163	Norm. χ^2	10.29

Table 11 – Average Experimental and Predicted Kick for E1 Winding

Winding Current (A)	Experimental Kick (rad)	Predicted Kick Before Fit (rad)	Predicted Kick After Fit (rad)	% Diff. Before Fit	% Diff. After Fit	Total Field (Main Magnet + Bump) Before Fit (T)	Total Field (Main Magnet + Bump) After Fit (T)
-400	$-1.276 \pm 0.008\times10^{-3}$	-1.410×10^{-3}	-1.321×10^{-3}	9.50	3.40	1.133	1.153
-200	$-6.27 \pm 0.06\times10^{-4}$	-6.94×10^{-4}	-6.530×10^{-4}	11.74	4.98	1.138	1.158
200	$6.22 \pm 0.08\times10^{-4}$	7.08×10^{-4}	6.299×10^{-4}	10.96	1.22	1.147	1.167
400	$1.256 \pm 0.008\times10^{-3}$	1.393×10^{-3}	1.222×10^{-3}	9.78	-2.74	1.151	1.171

Expected Main Magnet Current (A)	4836.43	Expected Main Magnet Field (T)	1.143	Norm. χ^2	243.86
Expected Main Magnet Current (A)	4948.39	Fitted Main Magnet Field (T)	1.163	Norm. χ^2	24.14

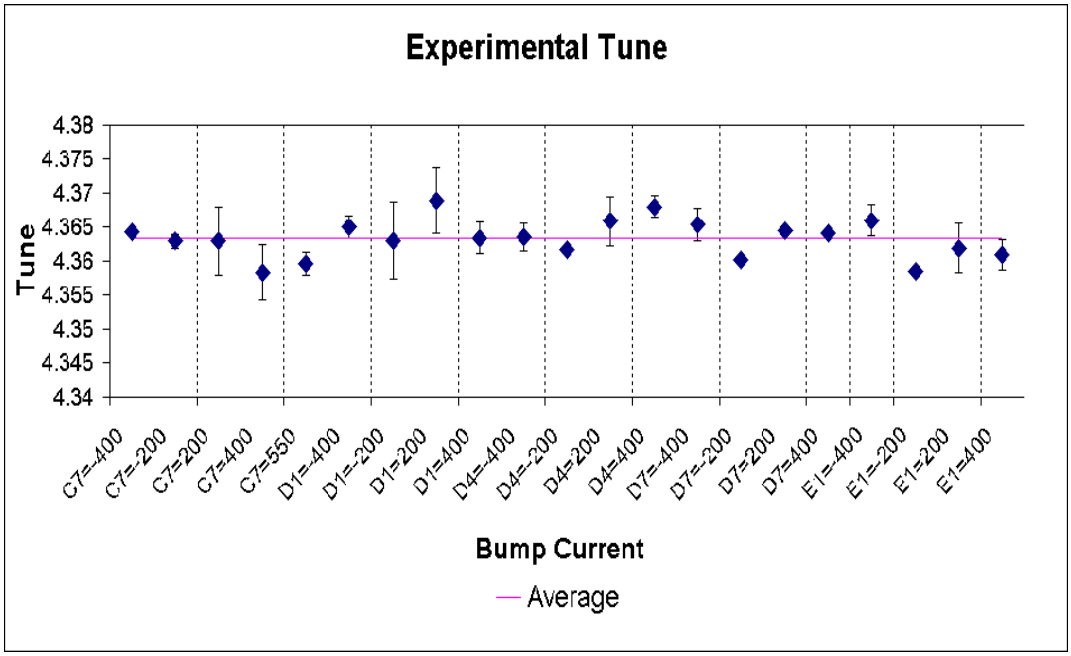

Figure 3 - Plot of tune obtained from fitting procedure.

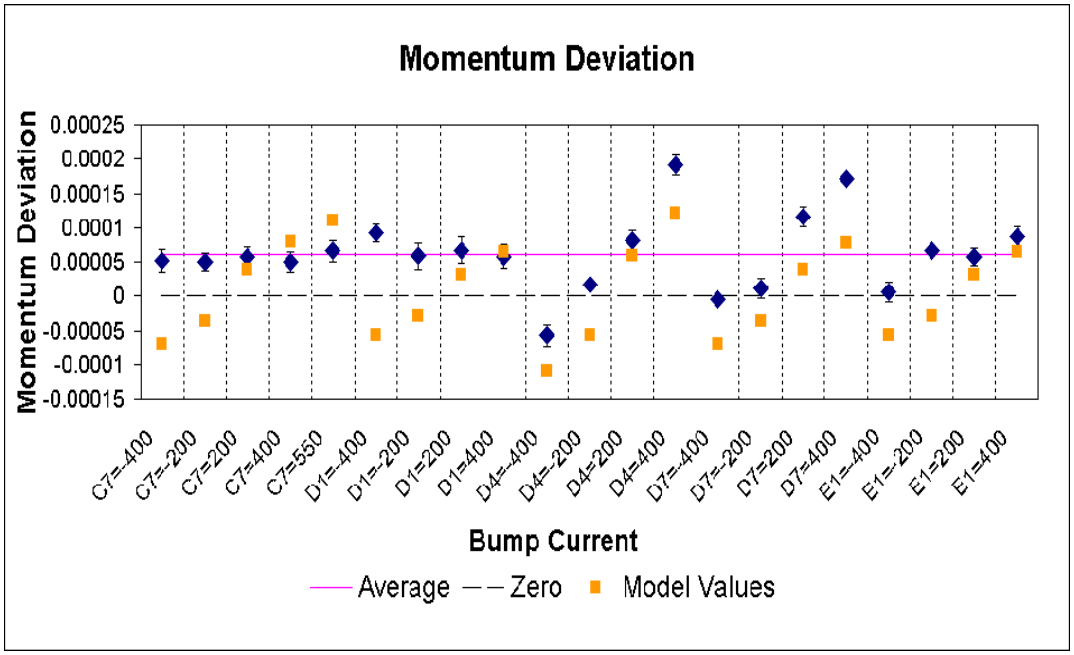

Figure 4 - Plot of momentum shift obtained from fitting procedure.

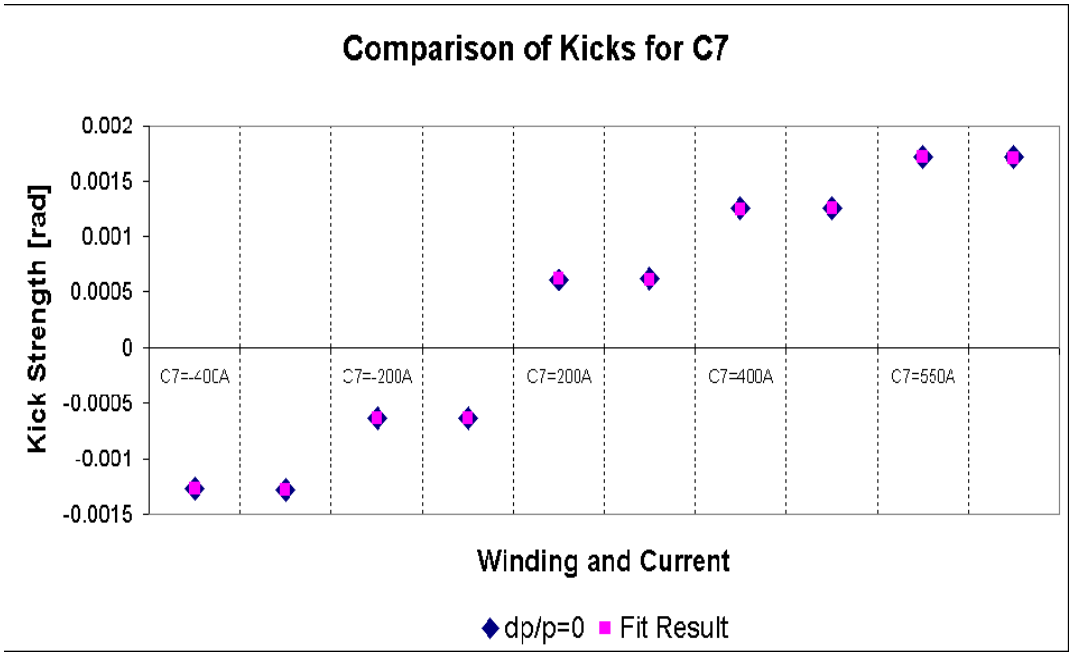

Figure 5 - Comparison of kicks when dp/p is set to zero and when used as a fitting parameter.

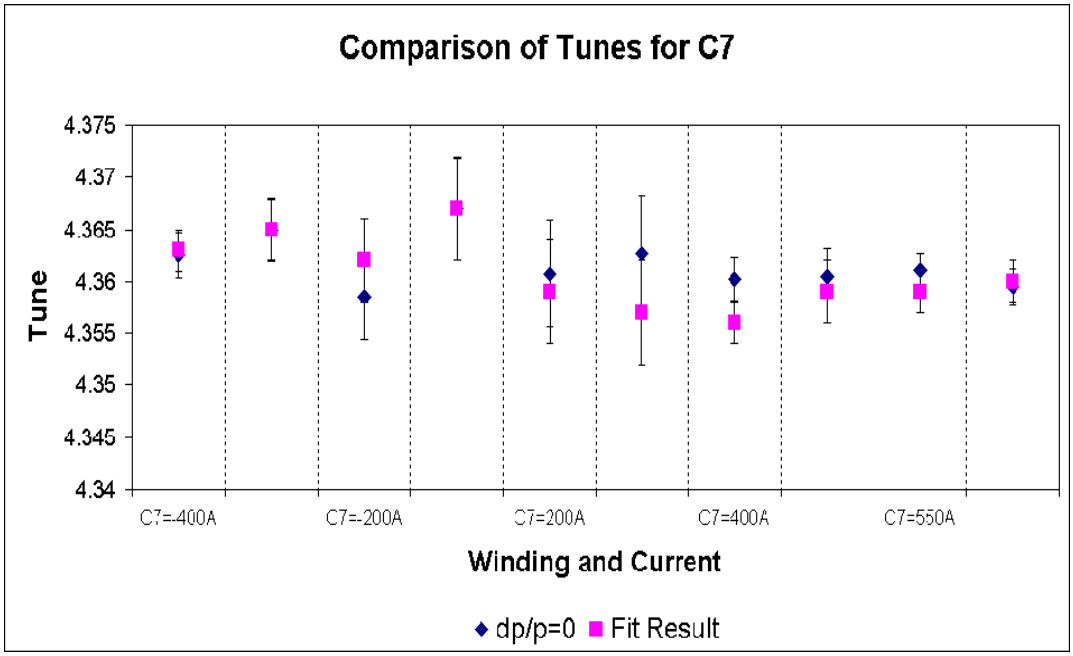

Figure 6 – Comparison of tunes when dp/p is set to zero and when used as a fitting parameter.

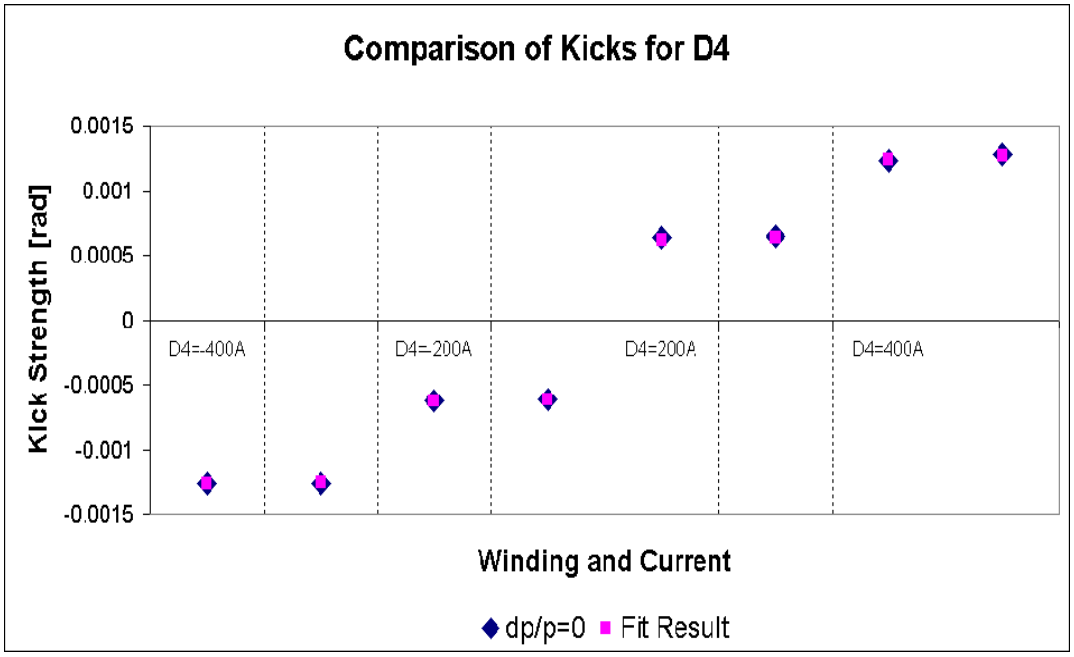

Figure 7 - Kicks for D4 winding when dp/p is set to zero and when used as a fitting parameter.

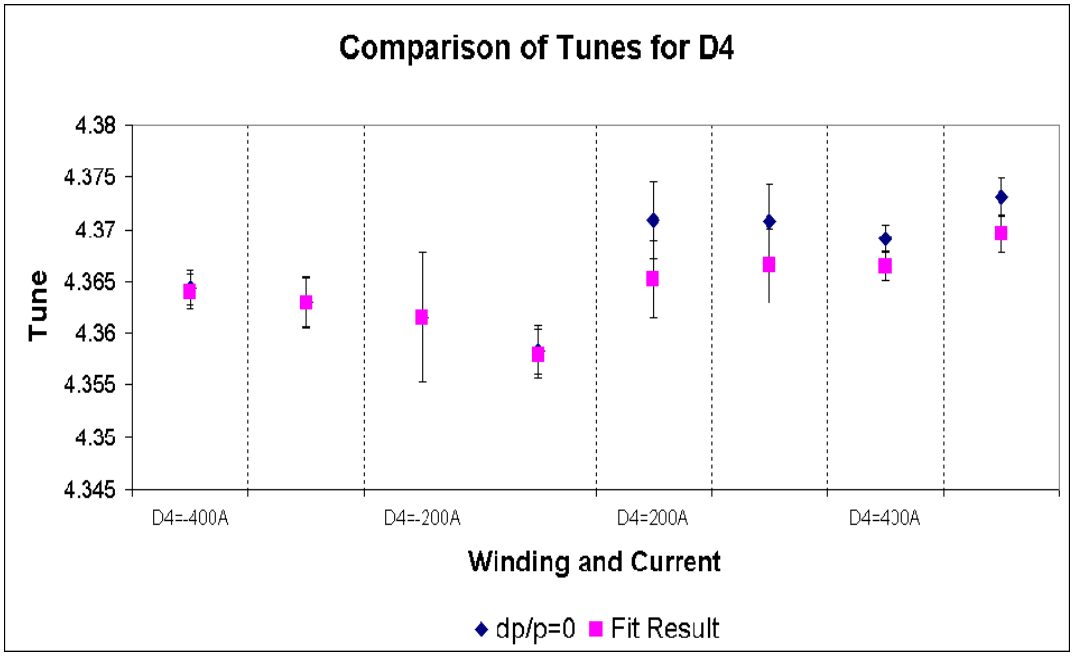

Figure 8 - Comparison of tunes when dp/p is set to zero and when used as a fitting parameter.

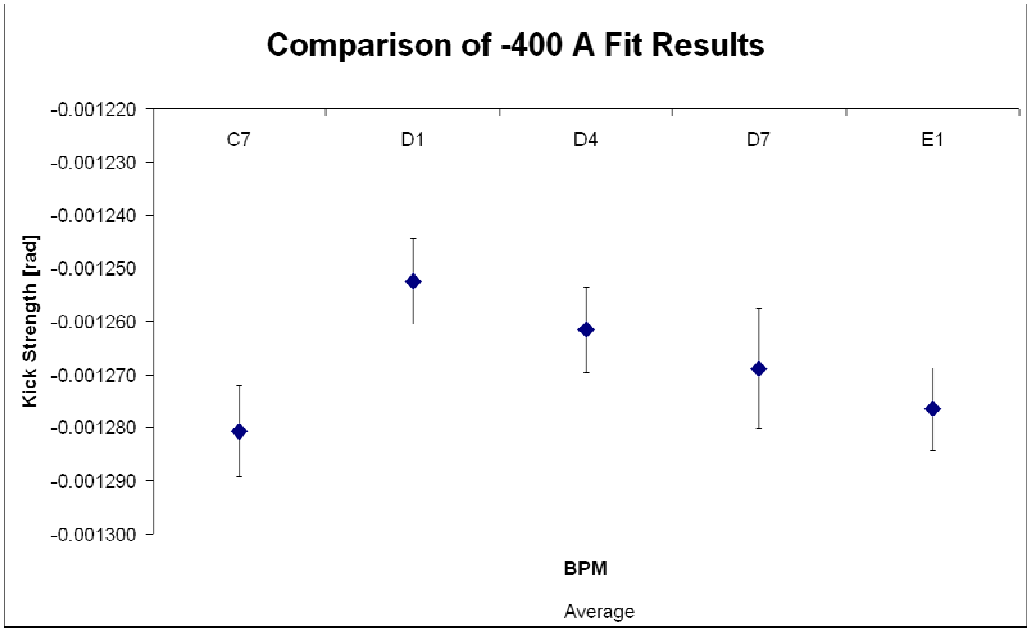

Figure 9

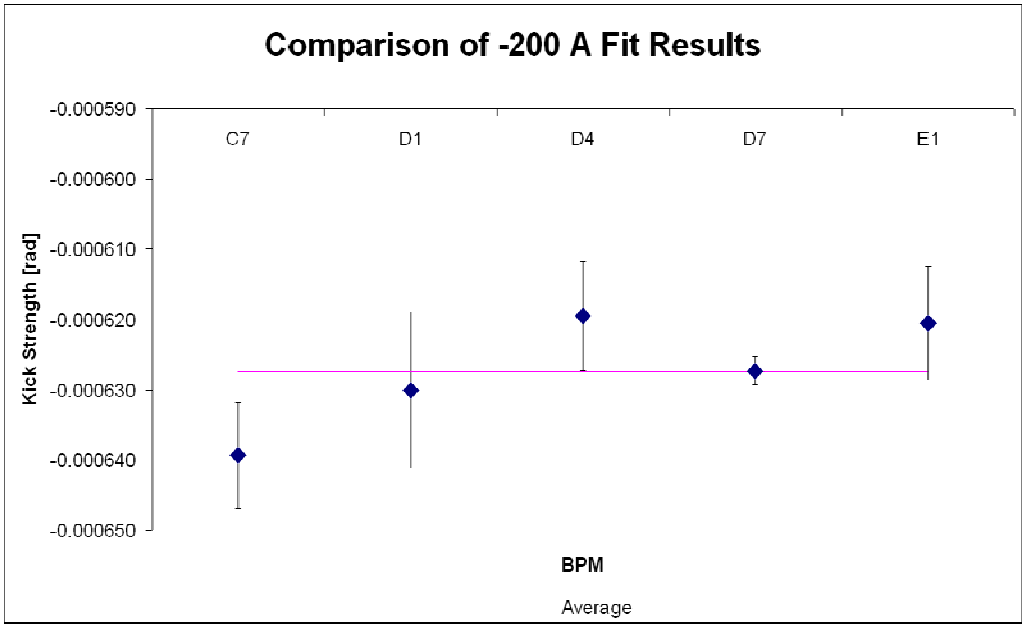

Figure 10

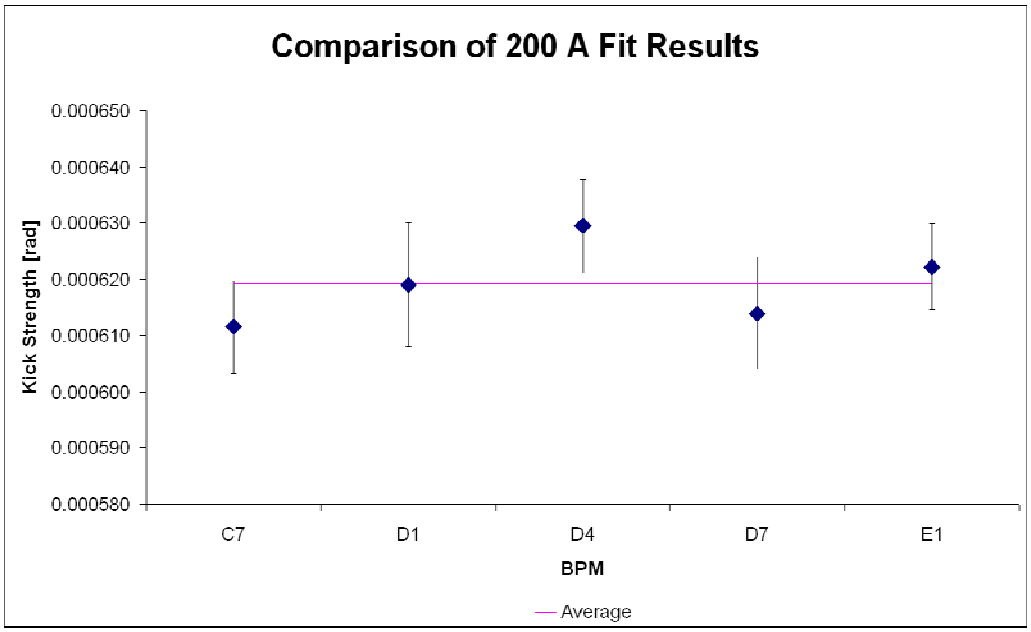

Figure 11

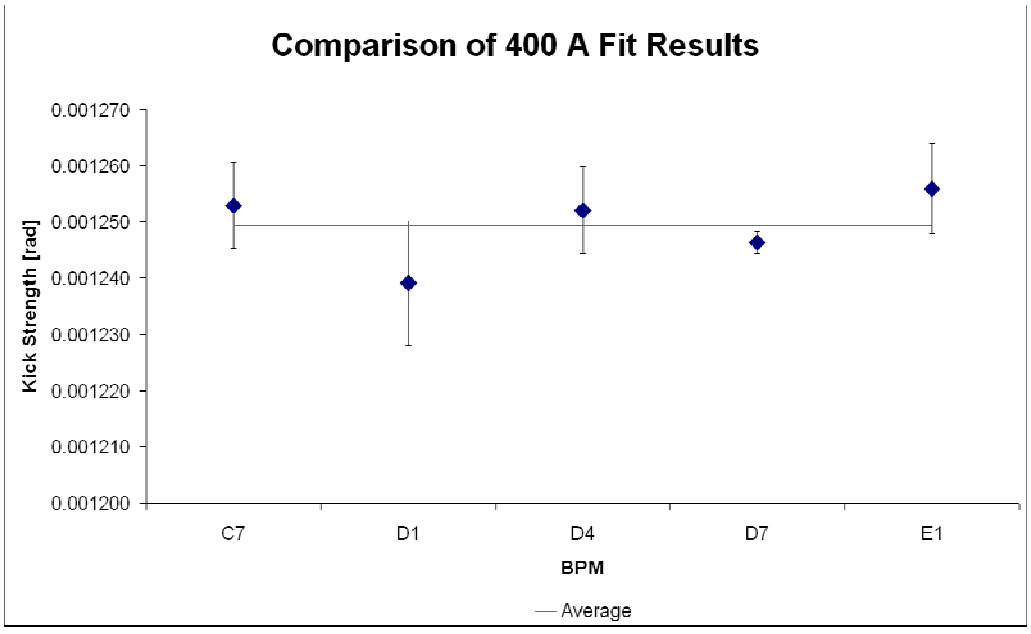

Figure 12

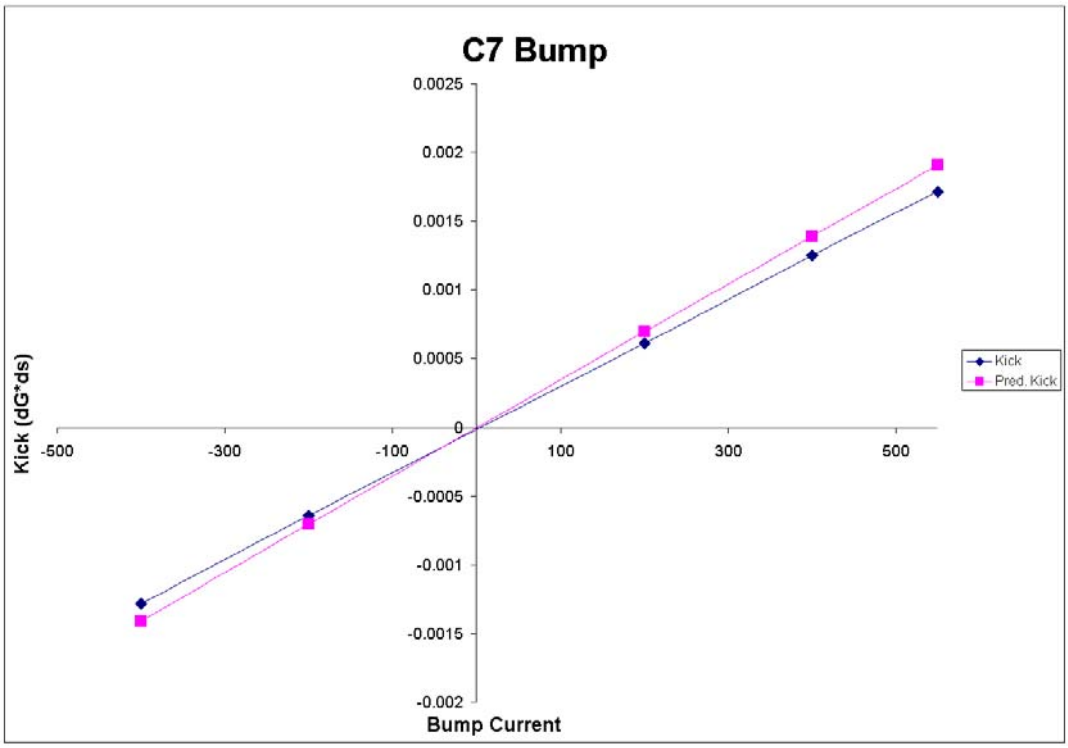

Figure 13 - Plot of Experimental and Predicted Kicks for C7 Winding.

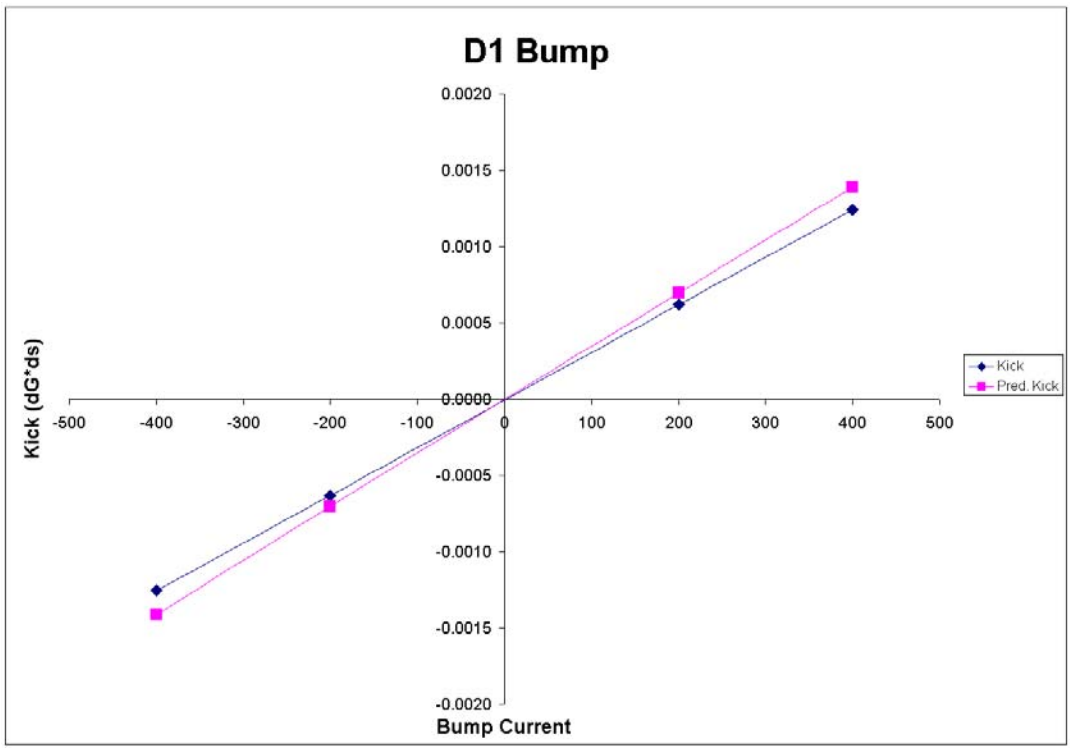

Figure 14 - Plot of Experimental and Predicted Kicks for D1 Winding.

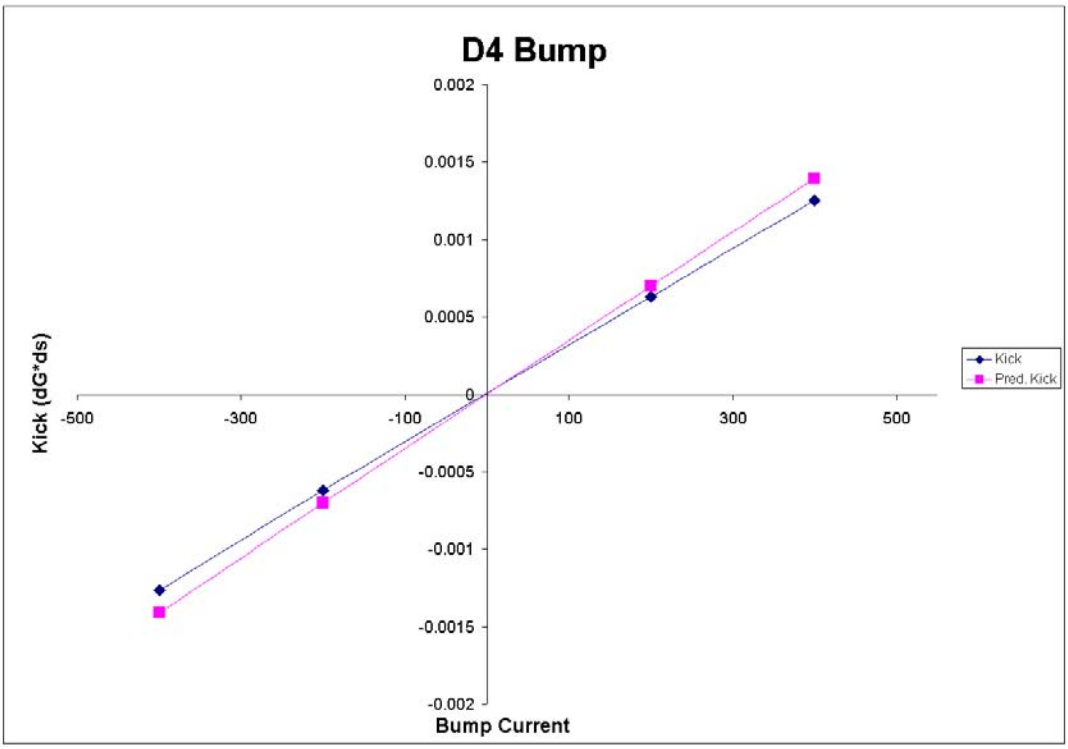

Figure 15 - Plot of Experimental and Predicted Kicks for D4 Winding.

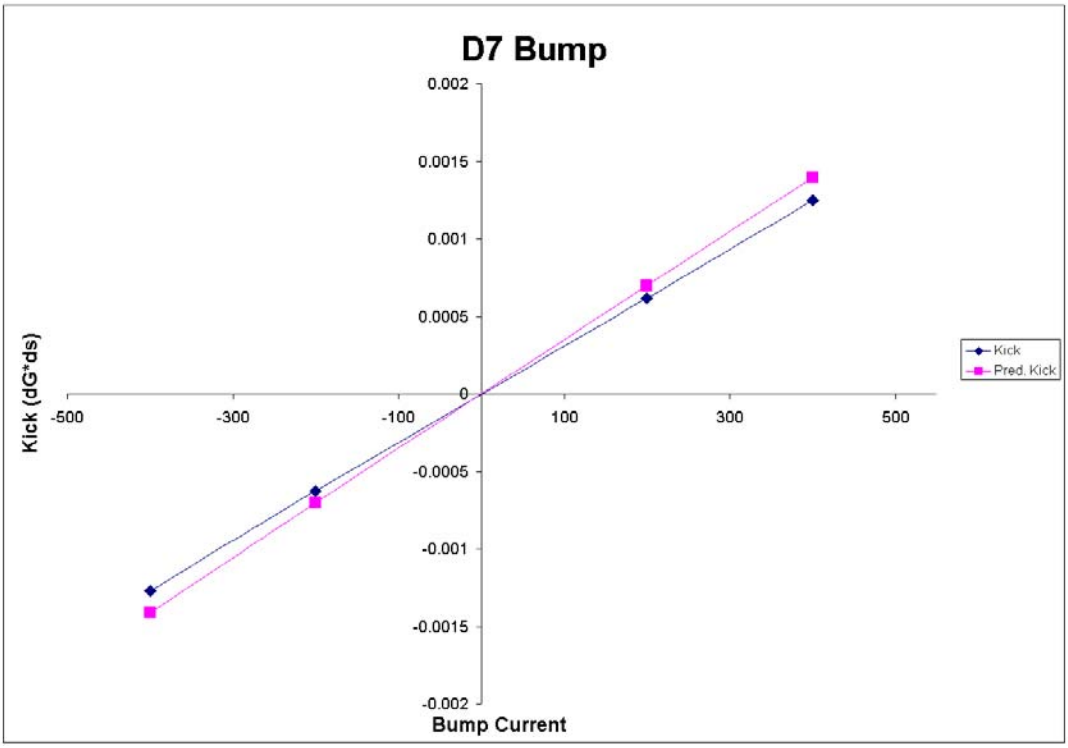

Figure 16 - Plot of Experimental and Predicted Kicks for D7 Winding.

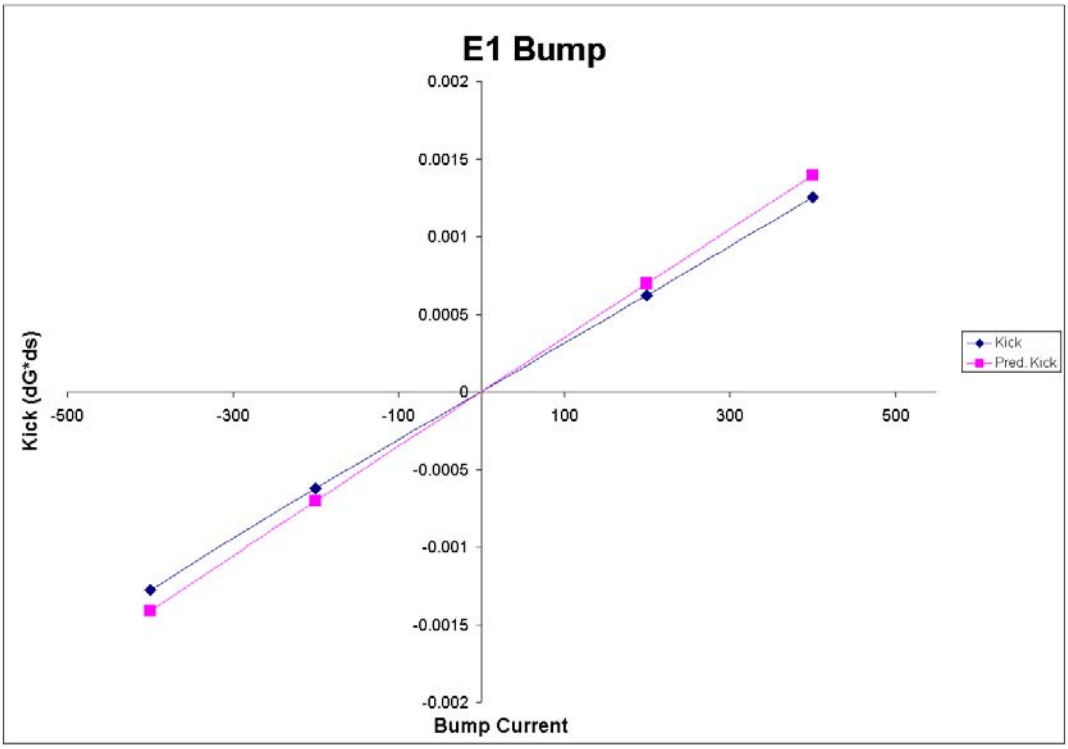

Figure 17 - Plot of Experimental and Predicted Kicks for E1 Winding.

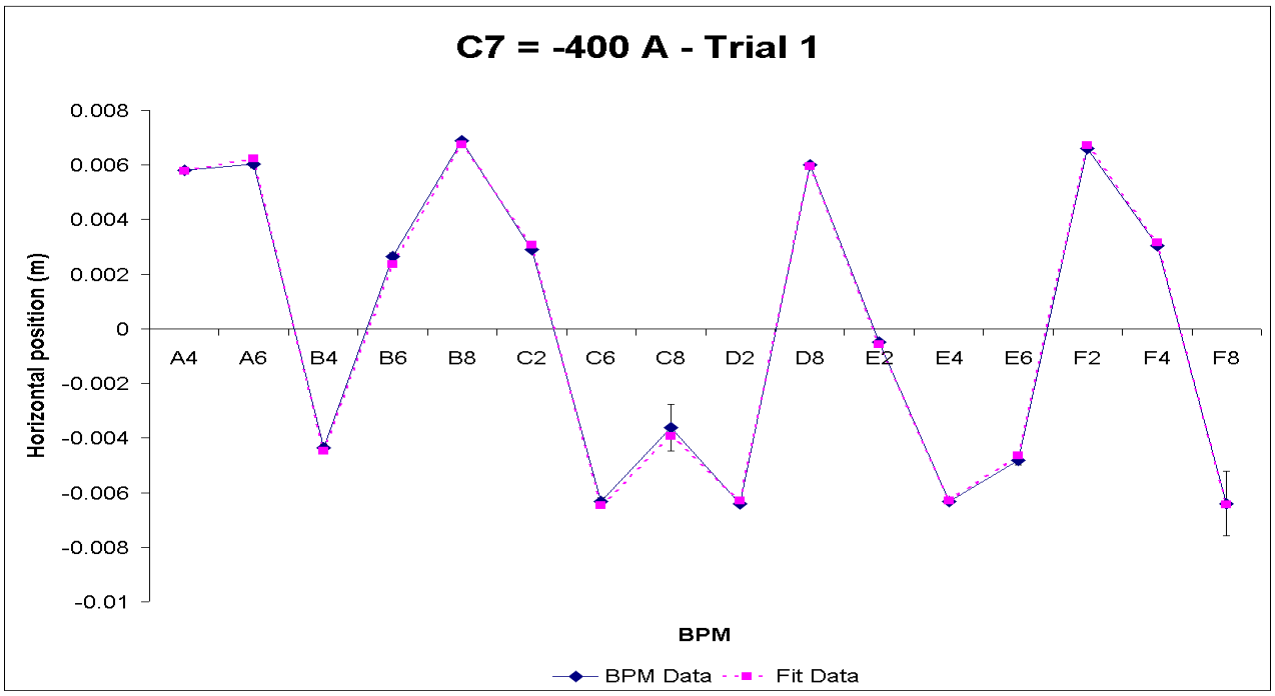

Figure 18

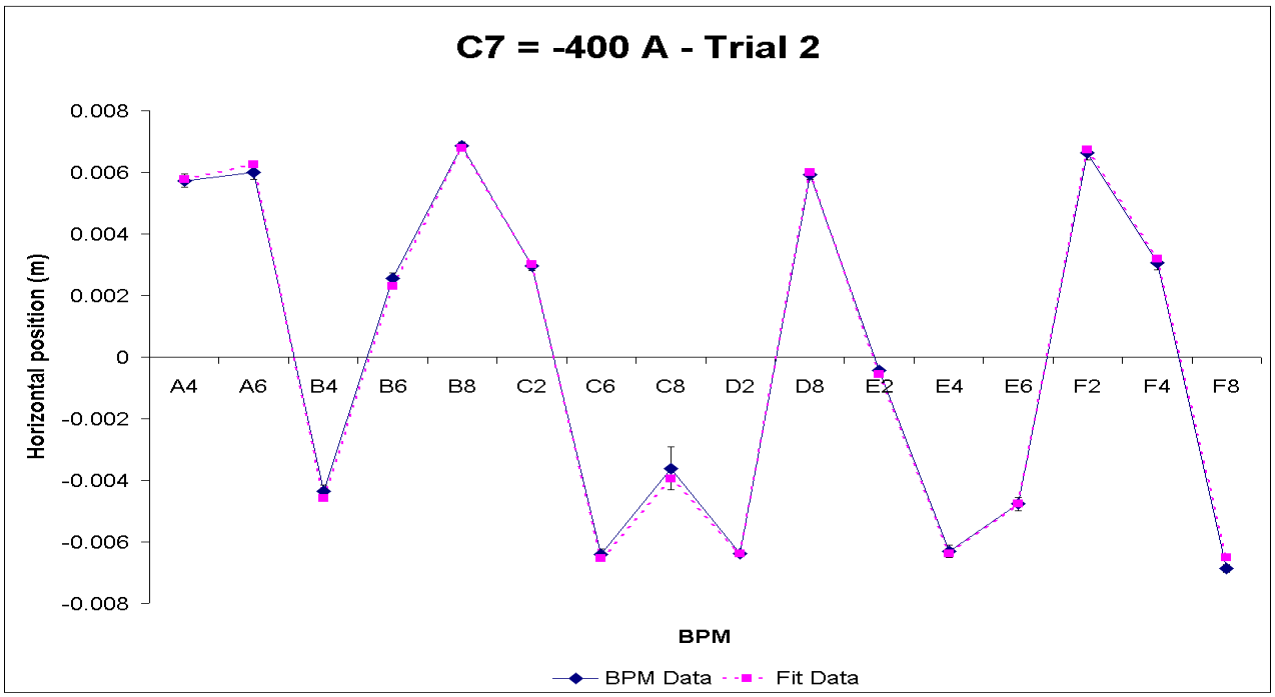

Figure 19

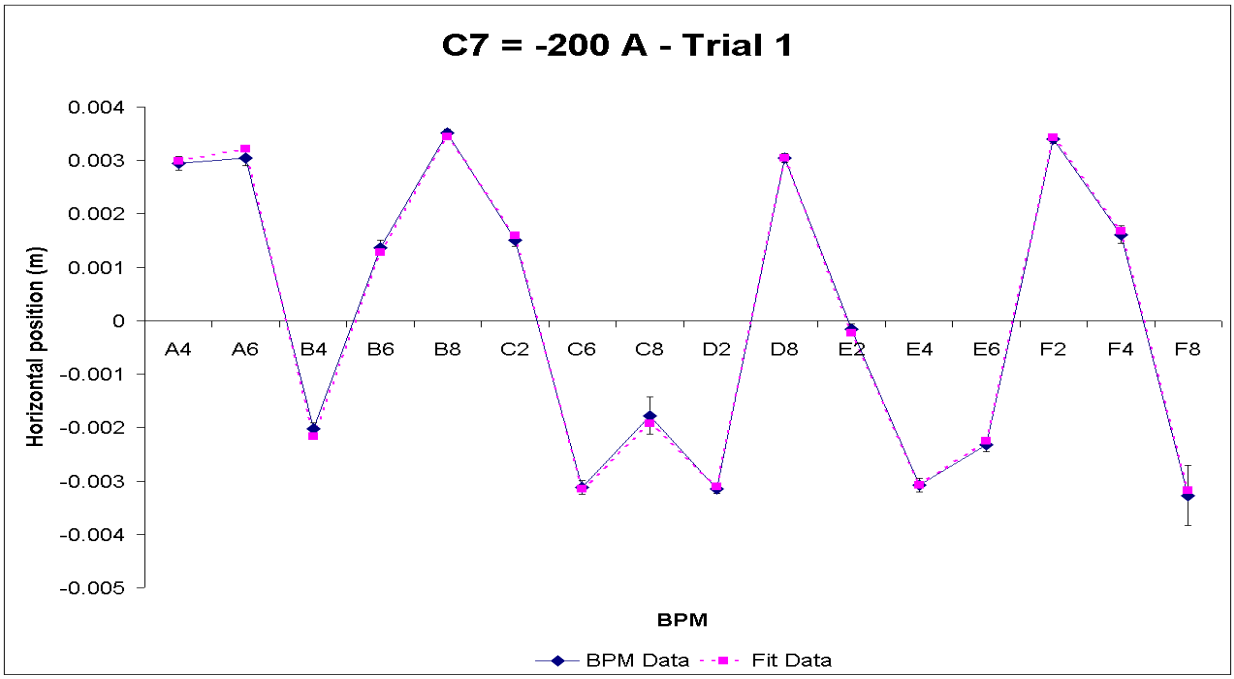

Figure 20

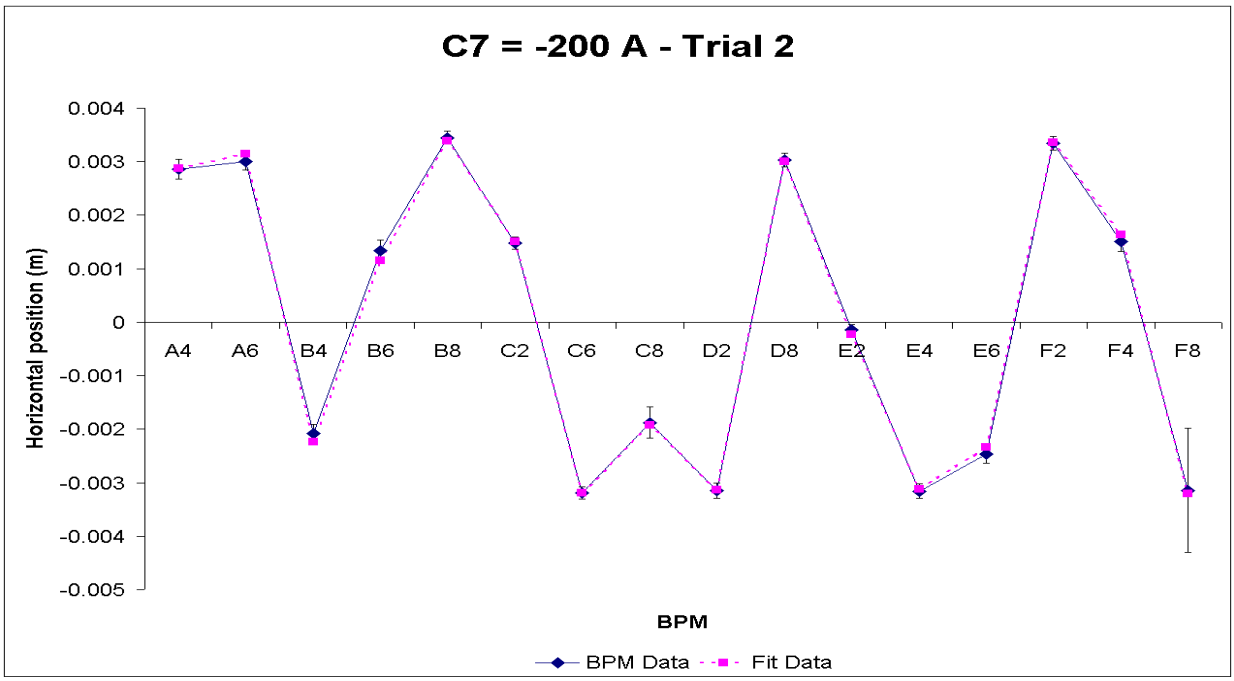

Figure 21

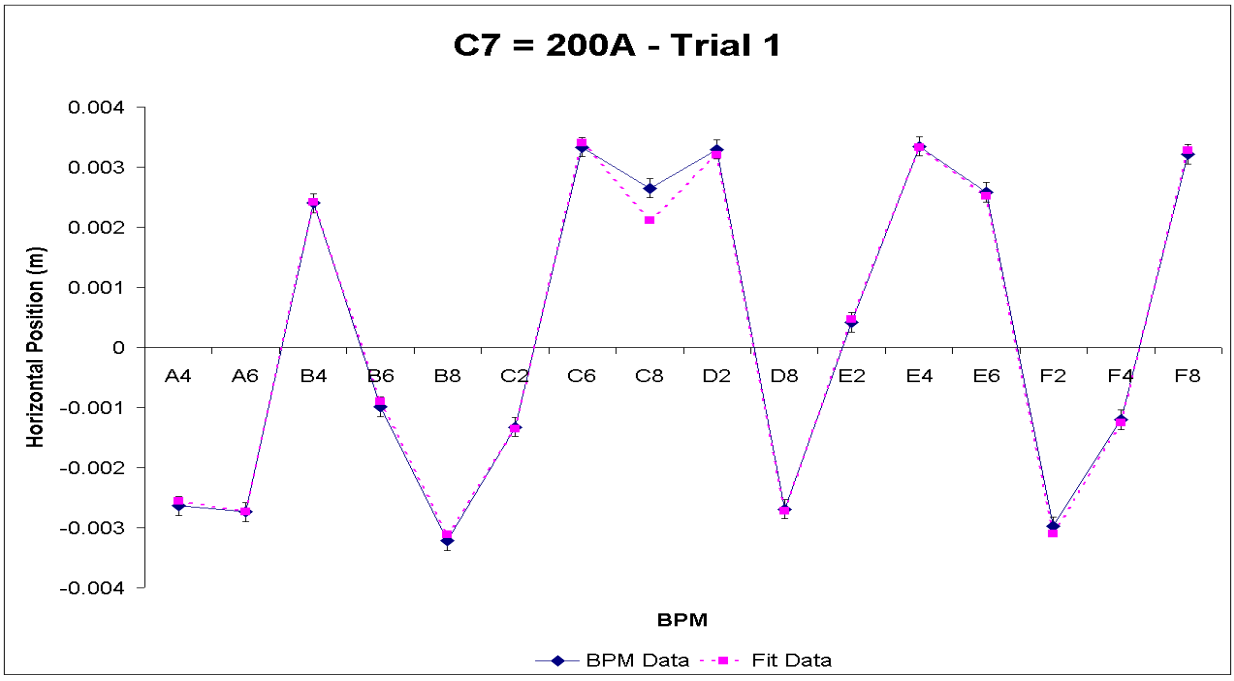

Figure 22

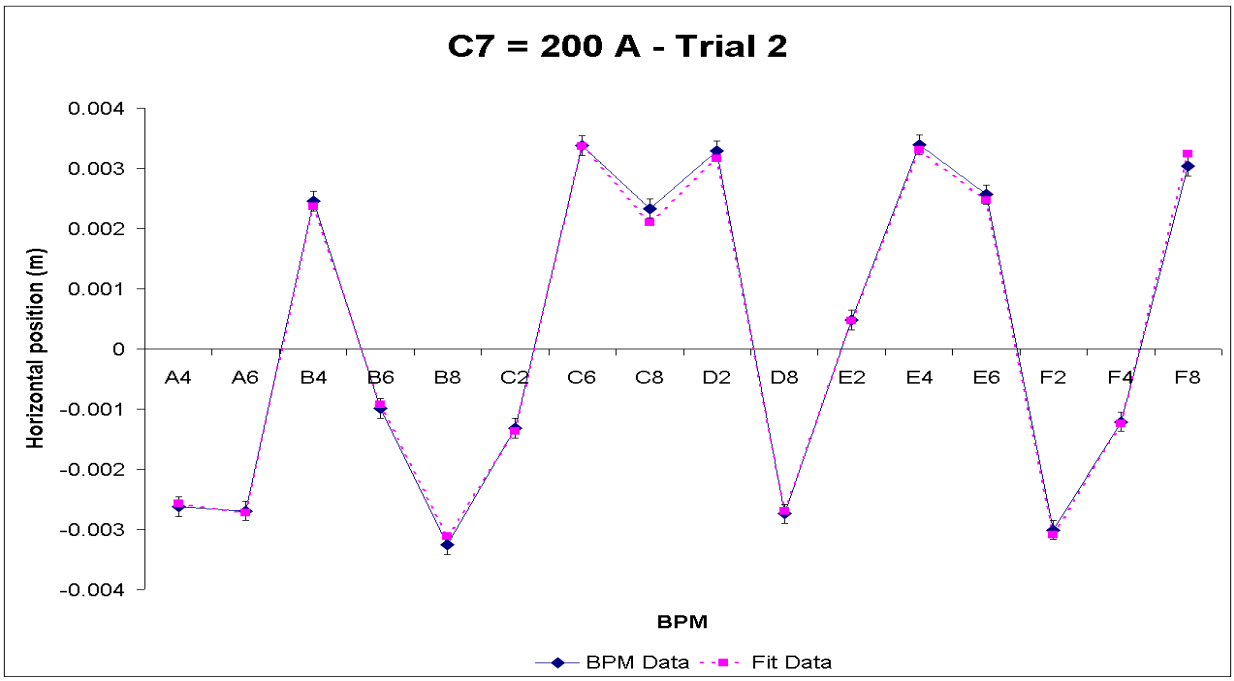

Figure 23

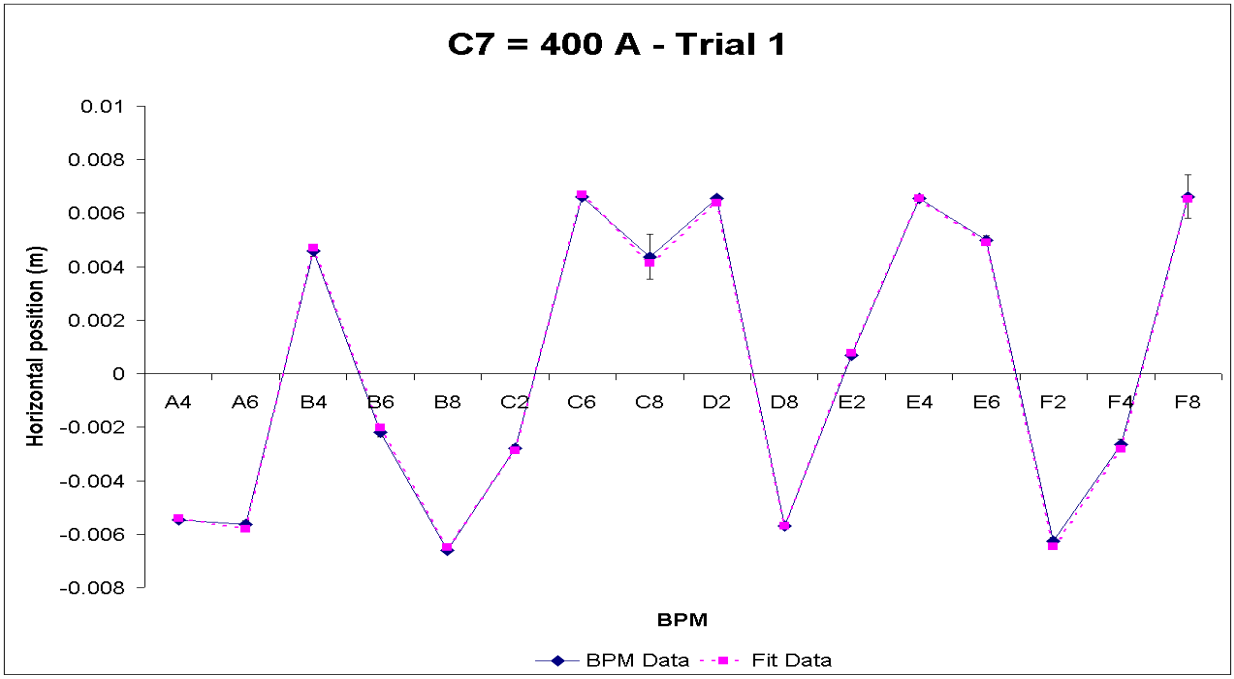

Figure 24

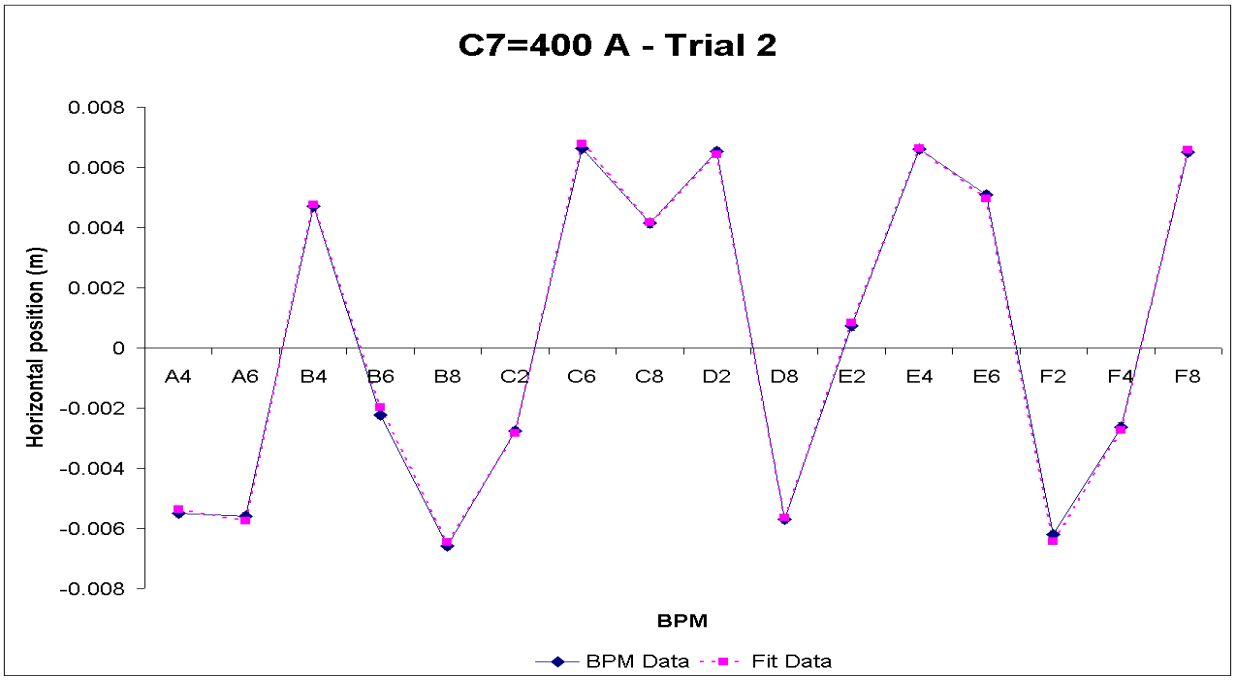

Figure 25

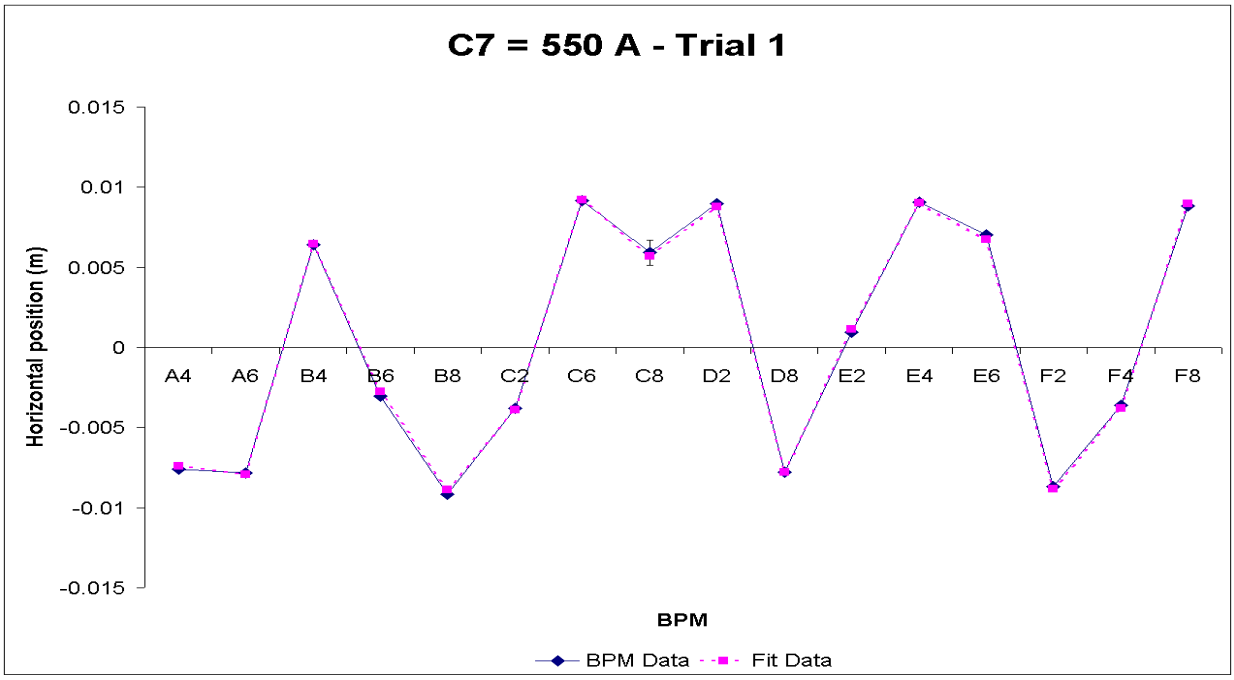

Figure 26

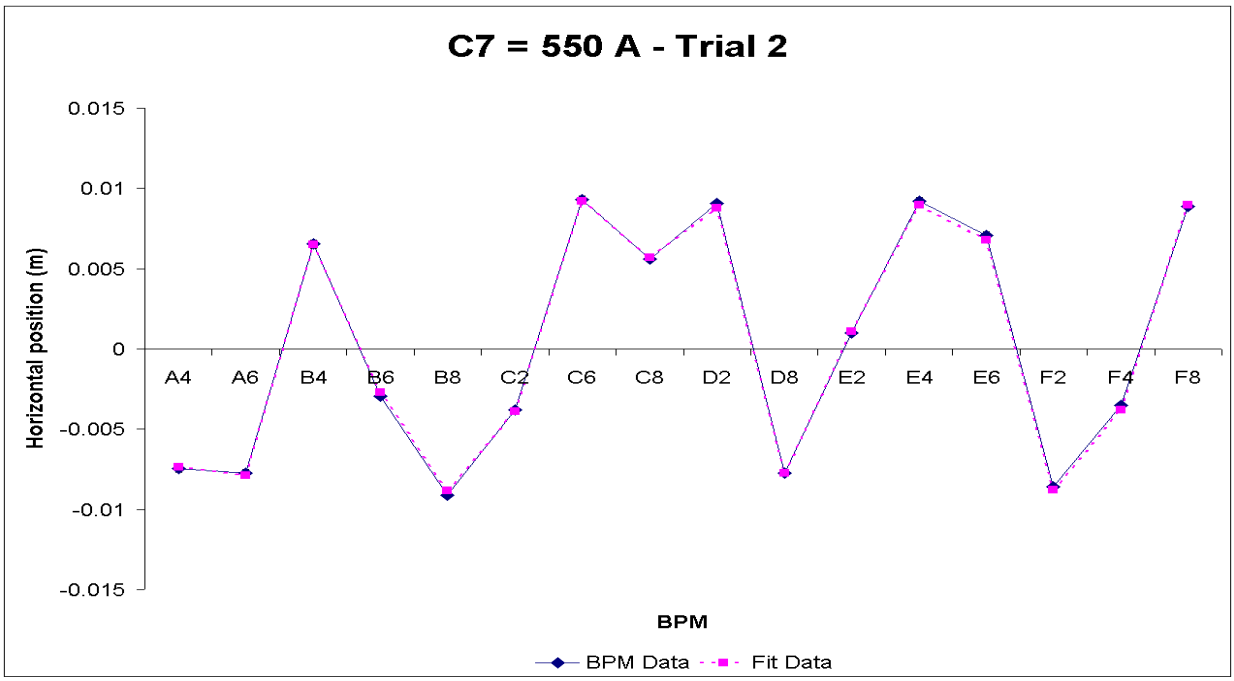

Figure 27

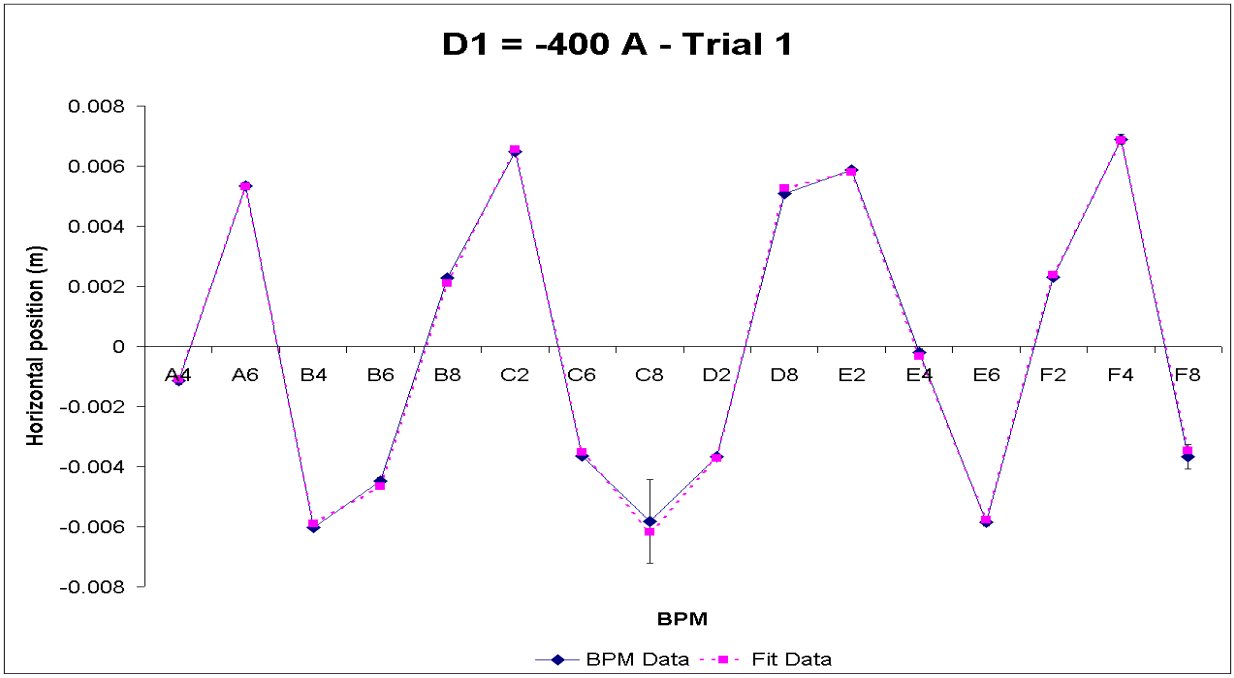

Figure 28

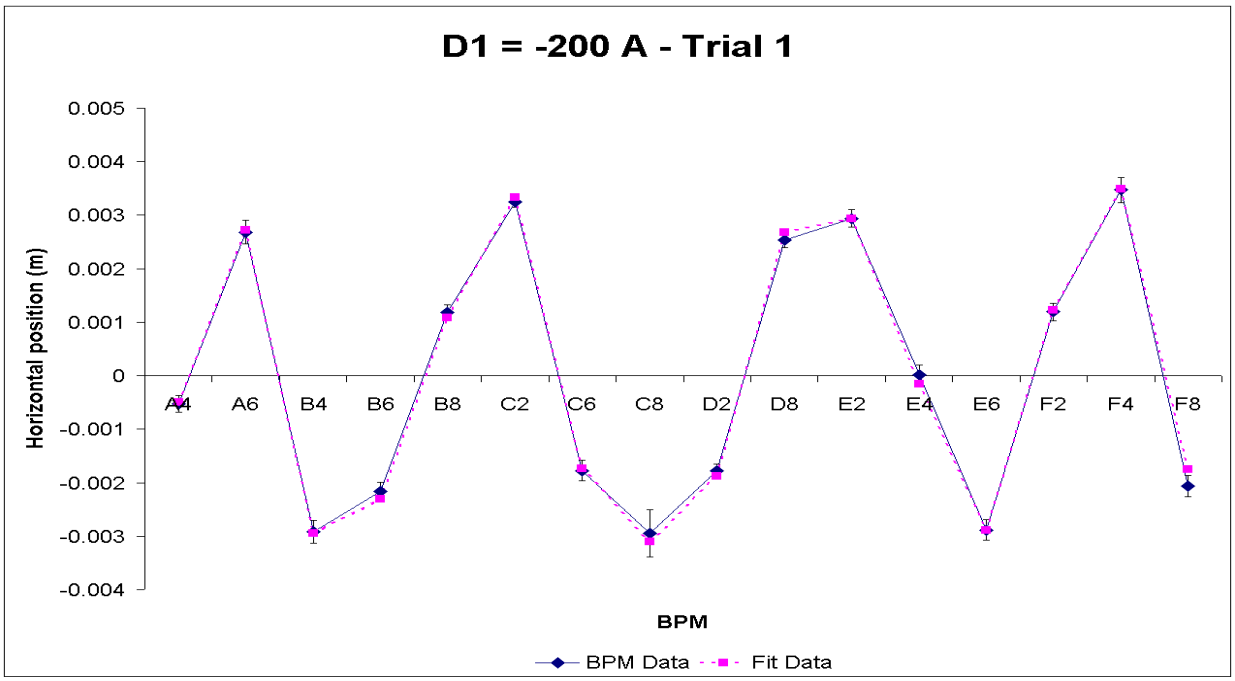

Figure 29

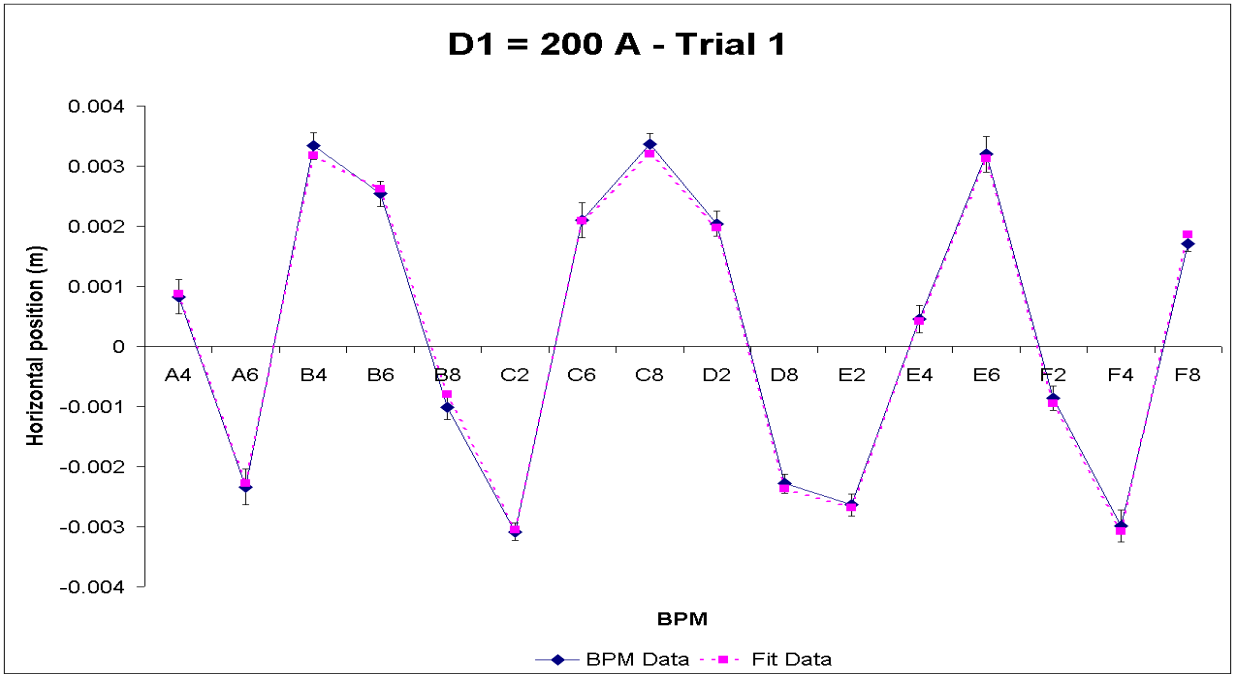

Figure 30

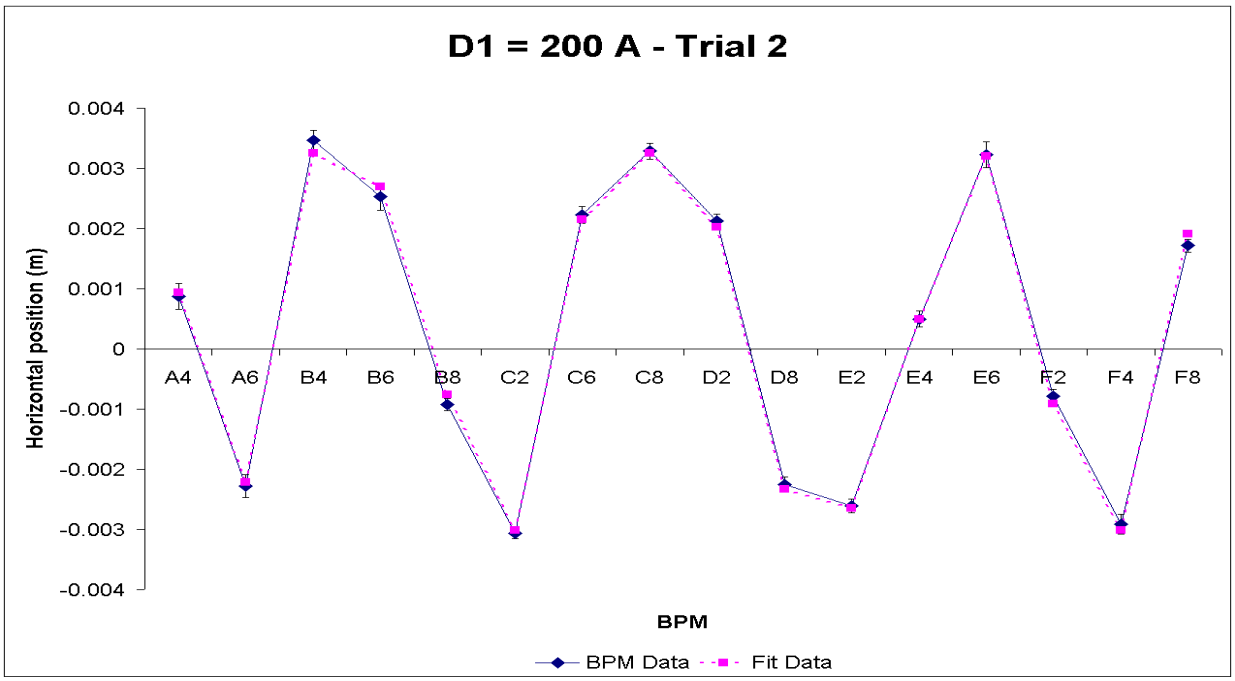

Figure 31

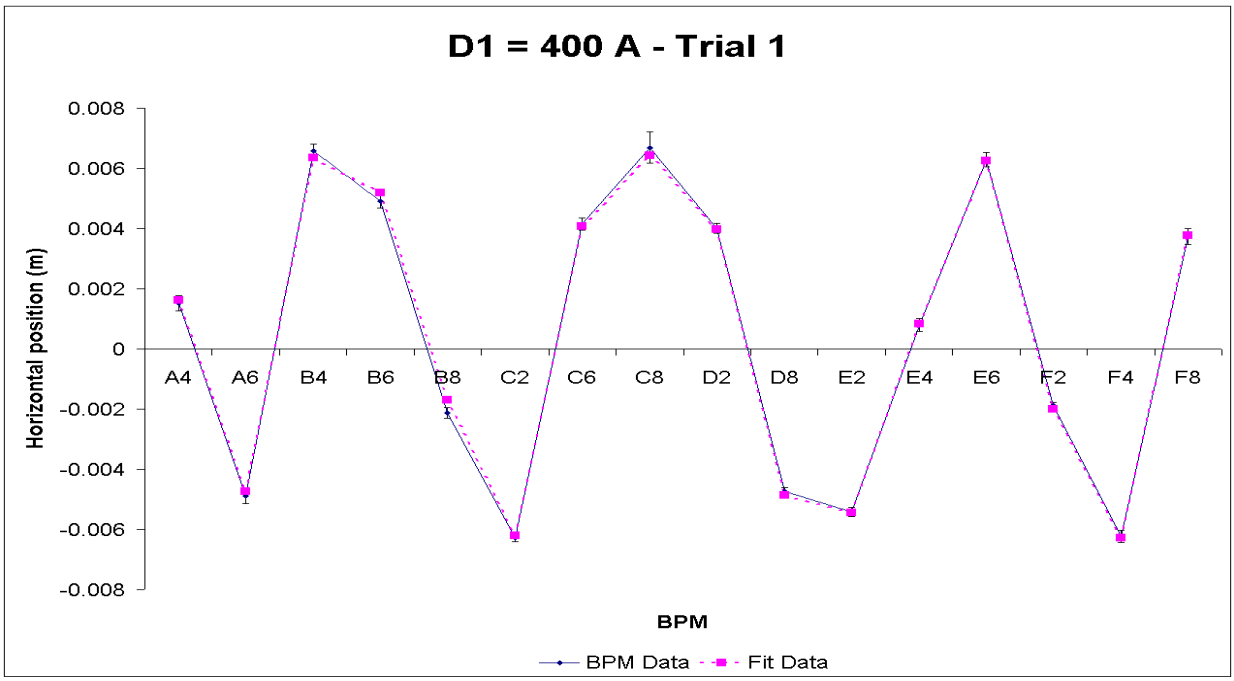

Figure 32

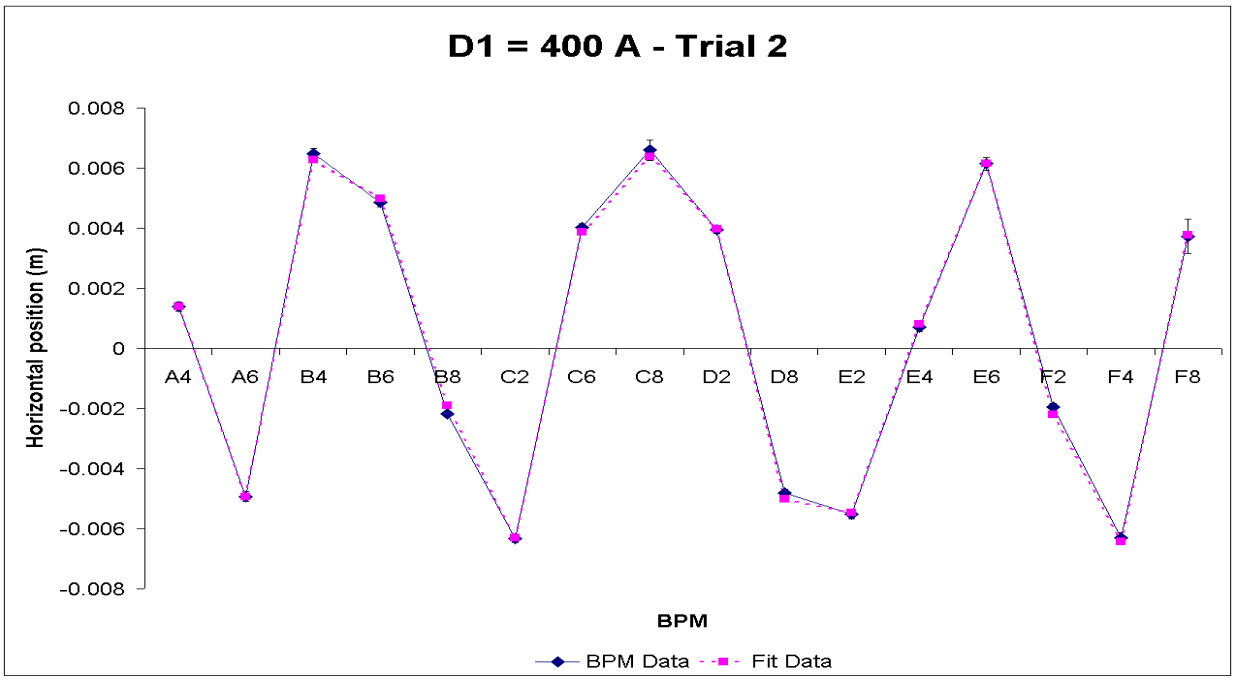

Figure 33

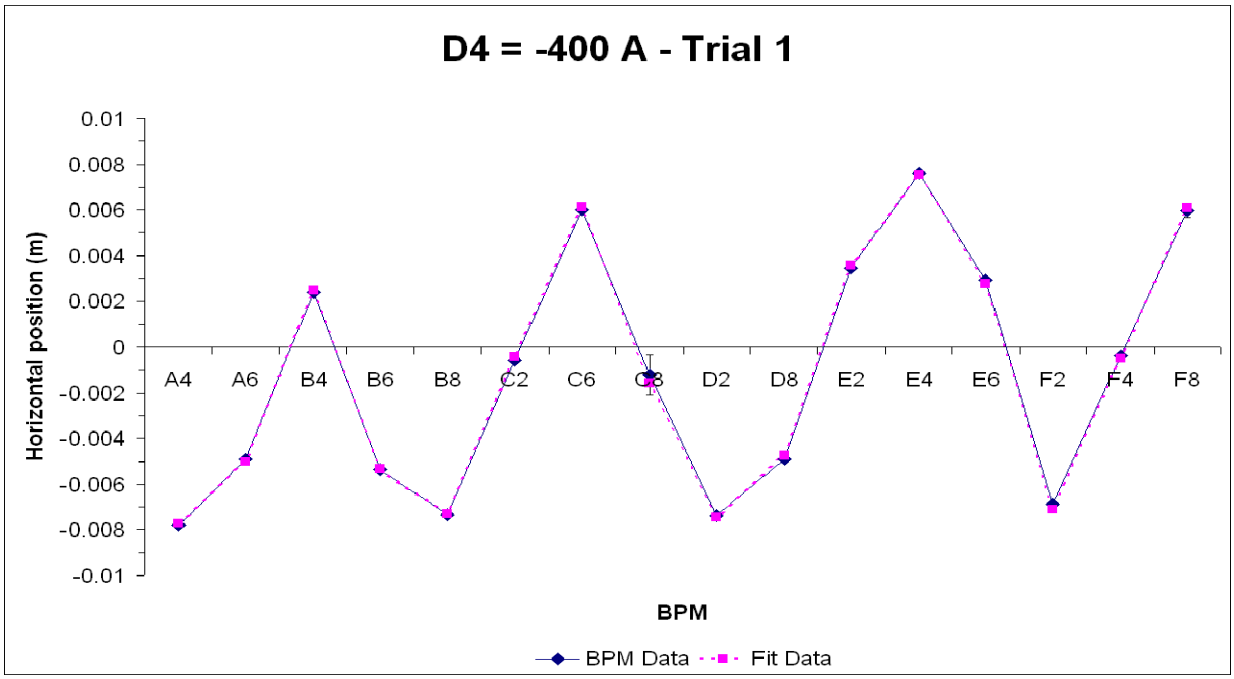

Figure 34

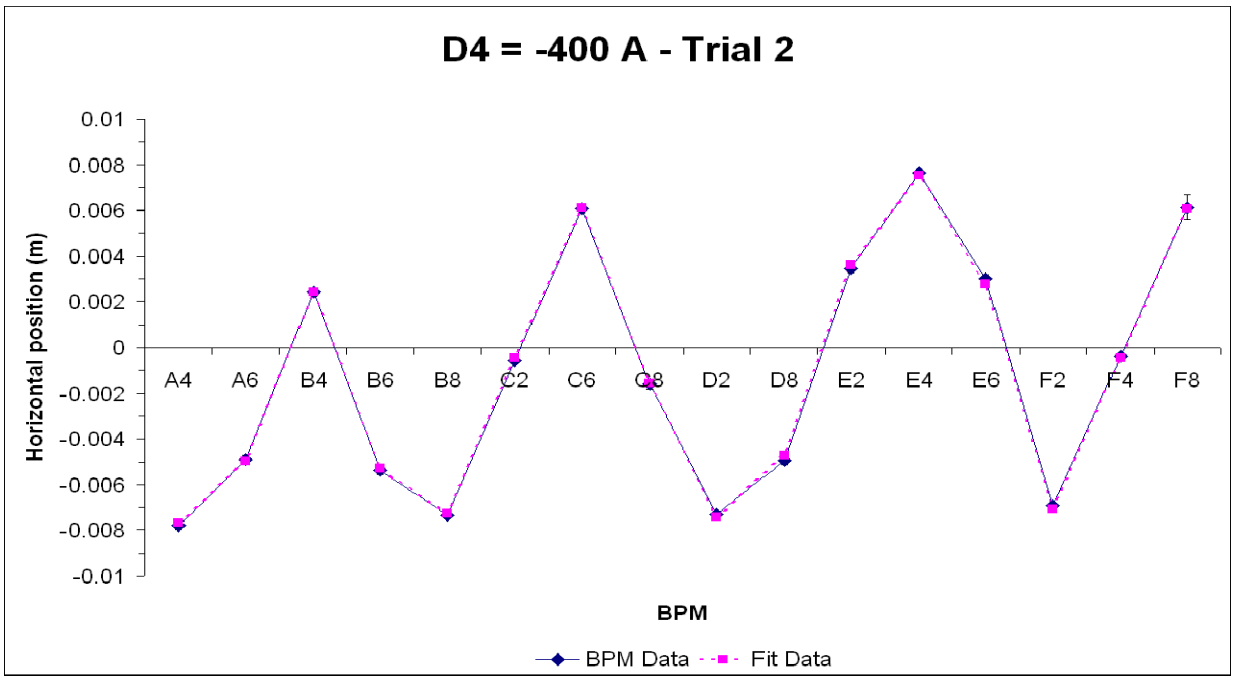

Figure 35

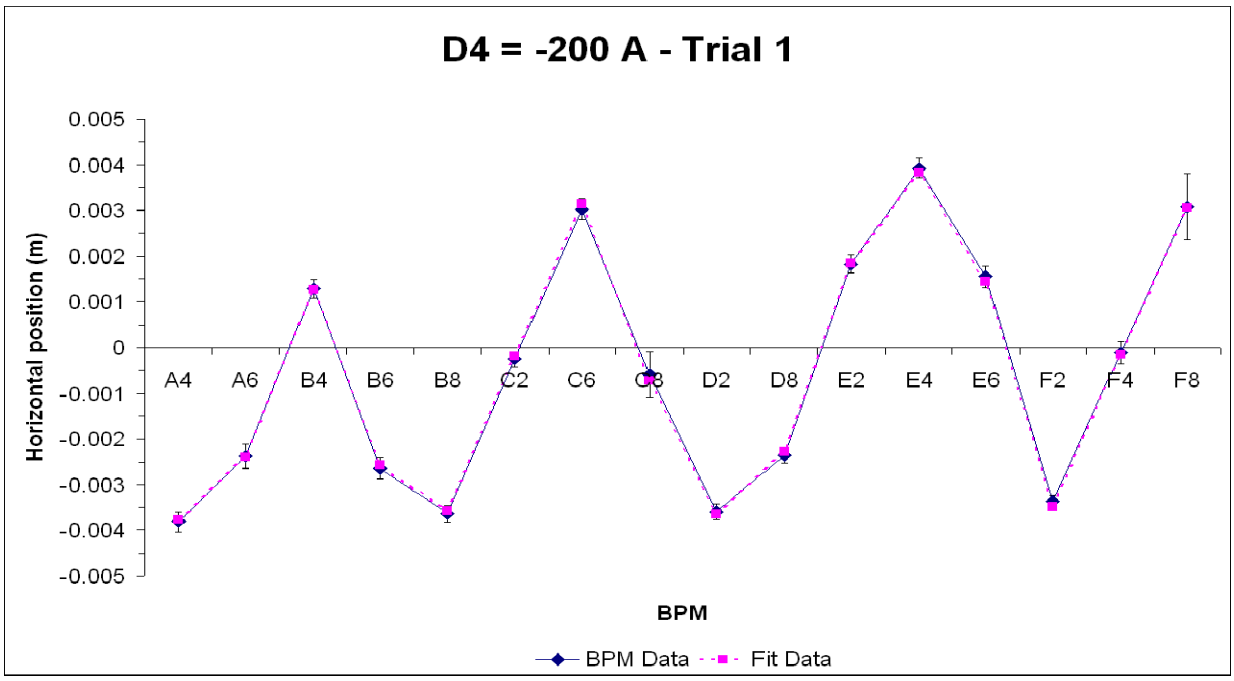

Figure 36

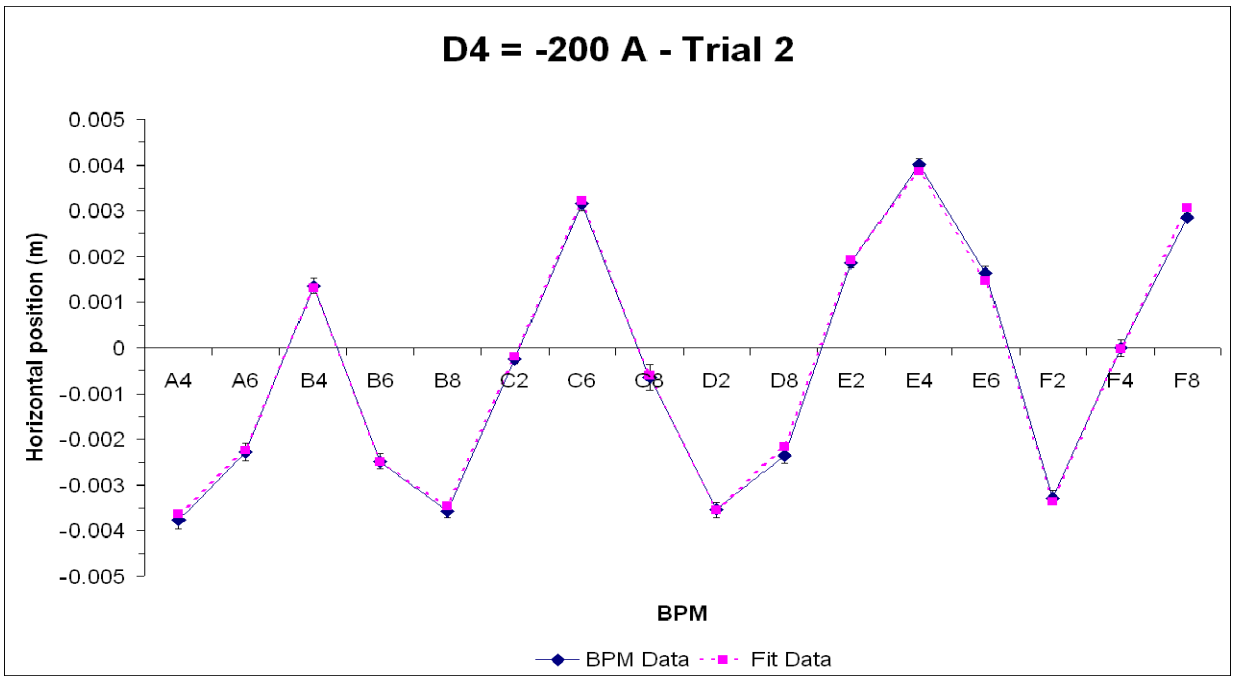

Figure 37

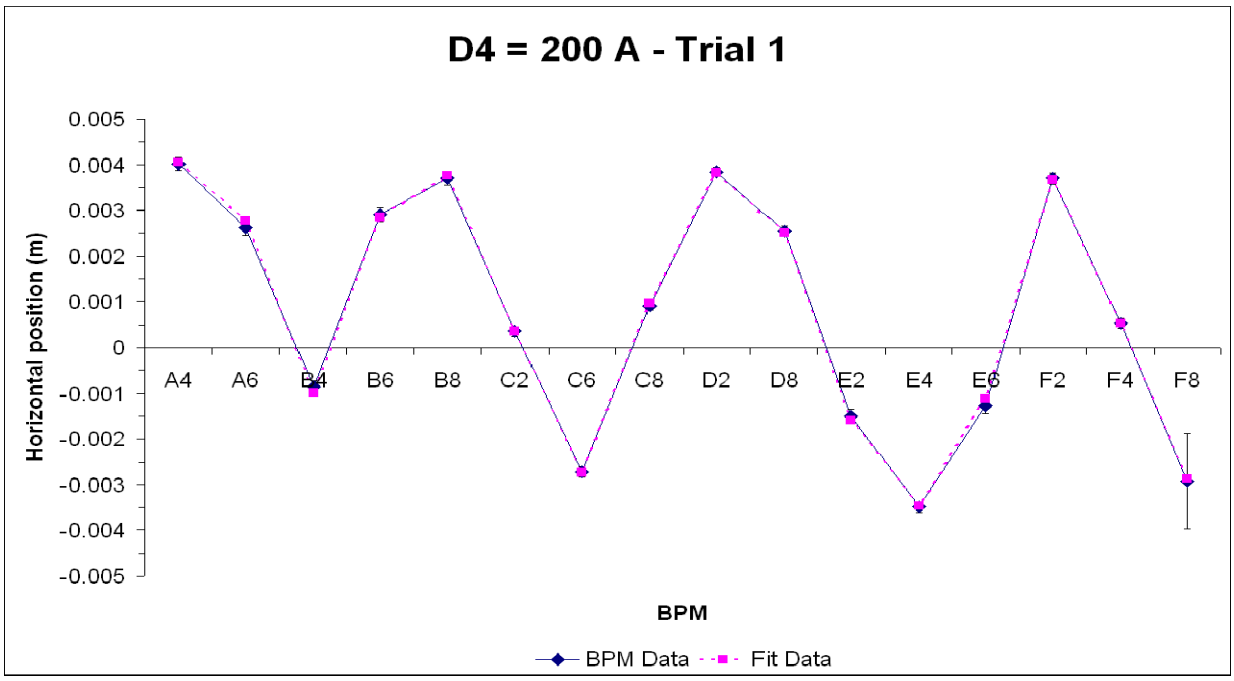

Figure 38

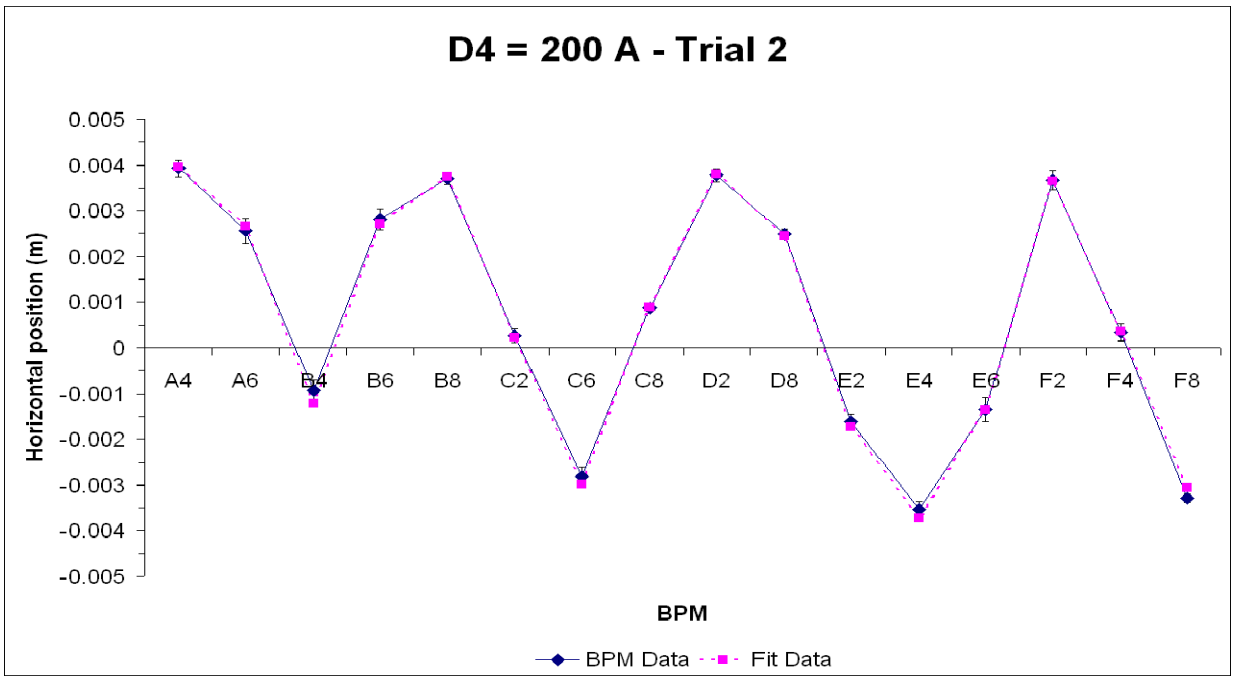

Figure 39

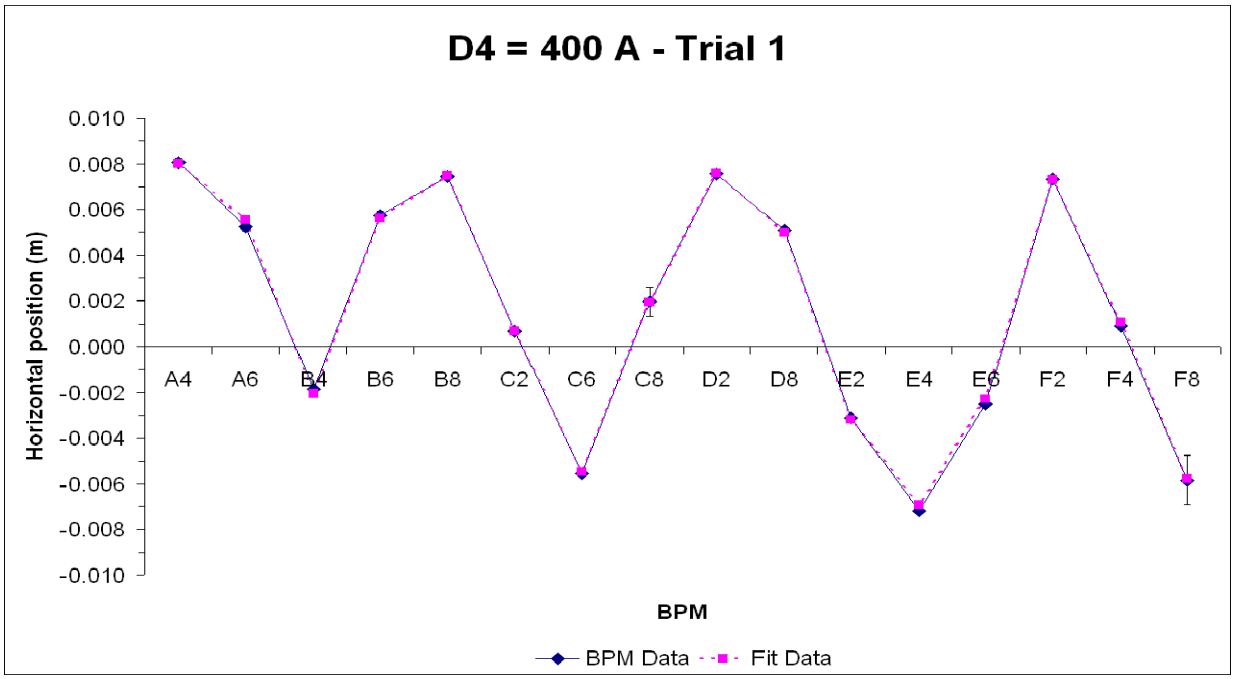

Figure 40

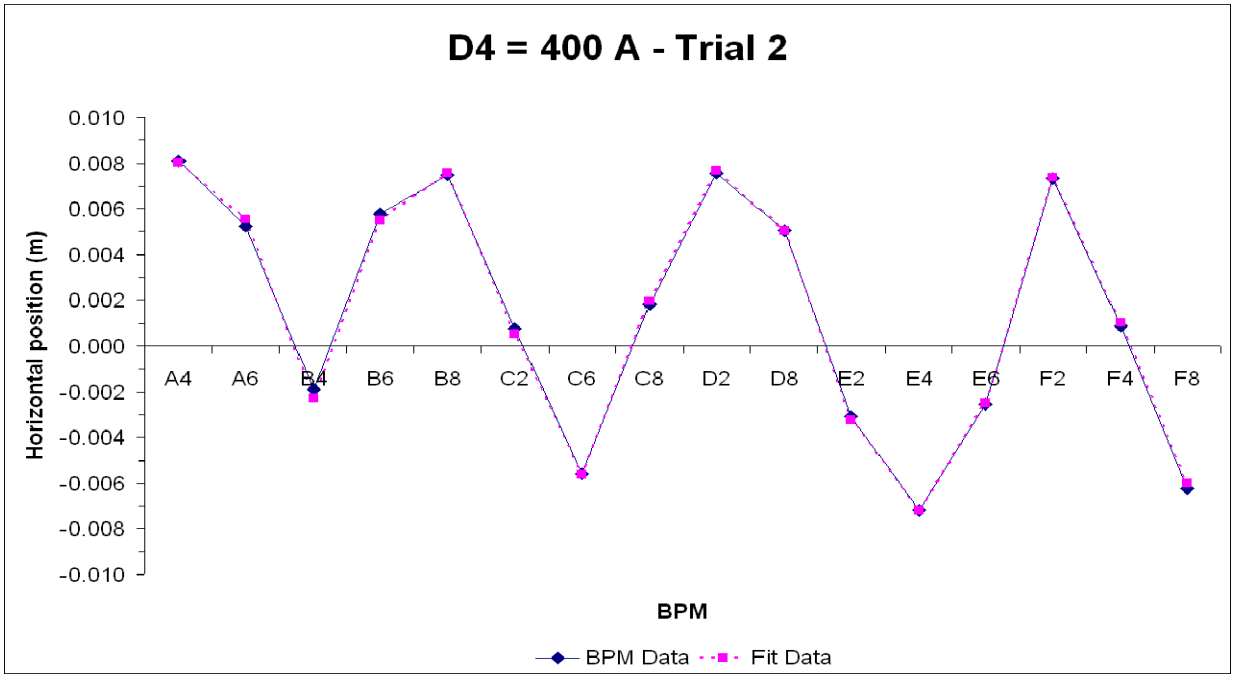

Figure 41

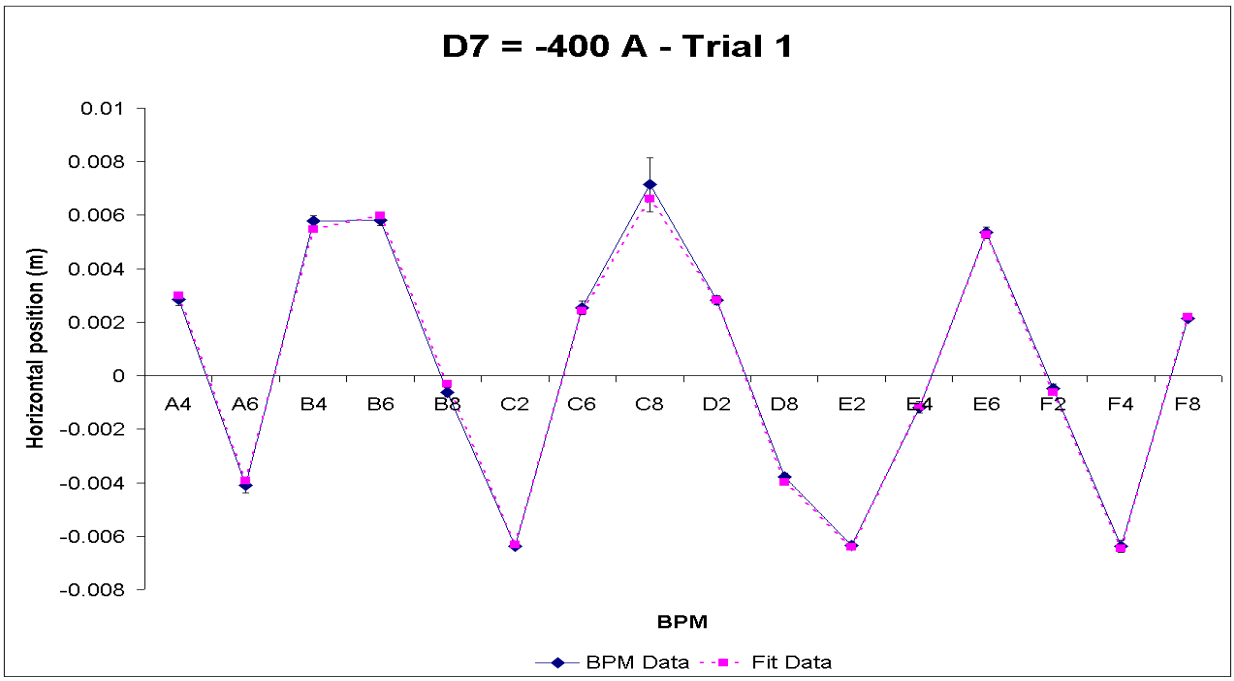

Figure 42

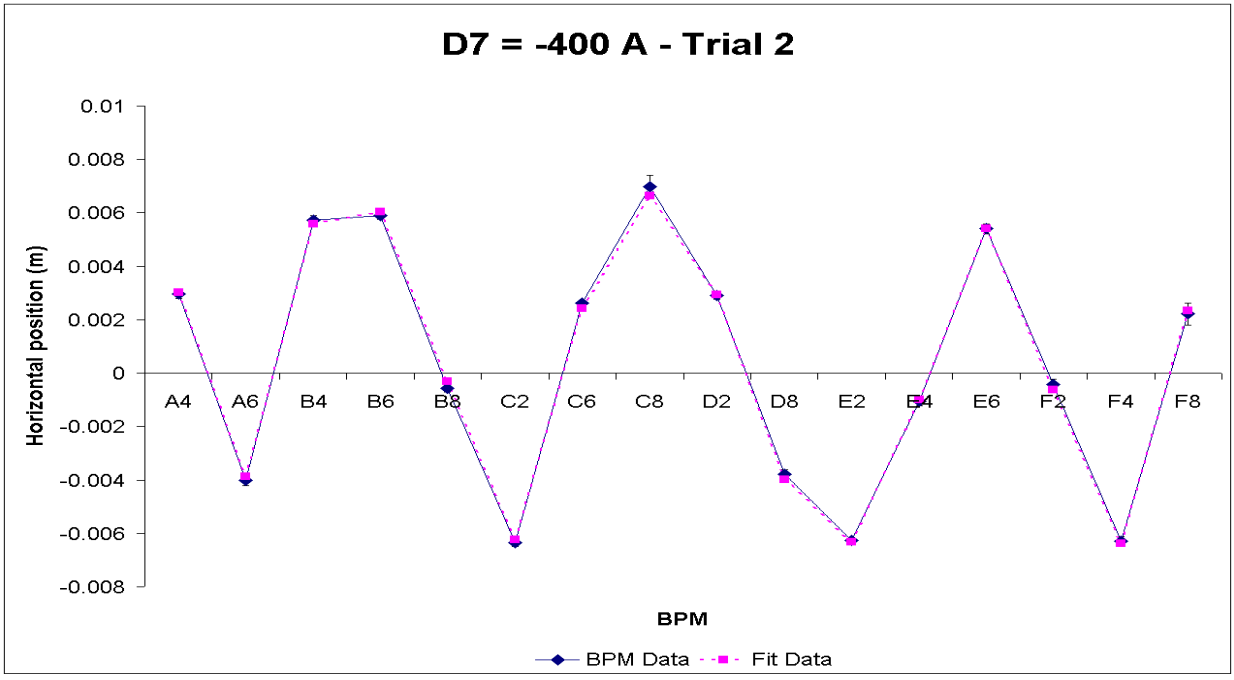

Figure 43

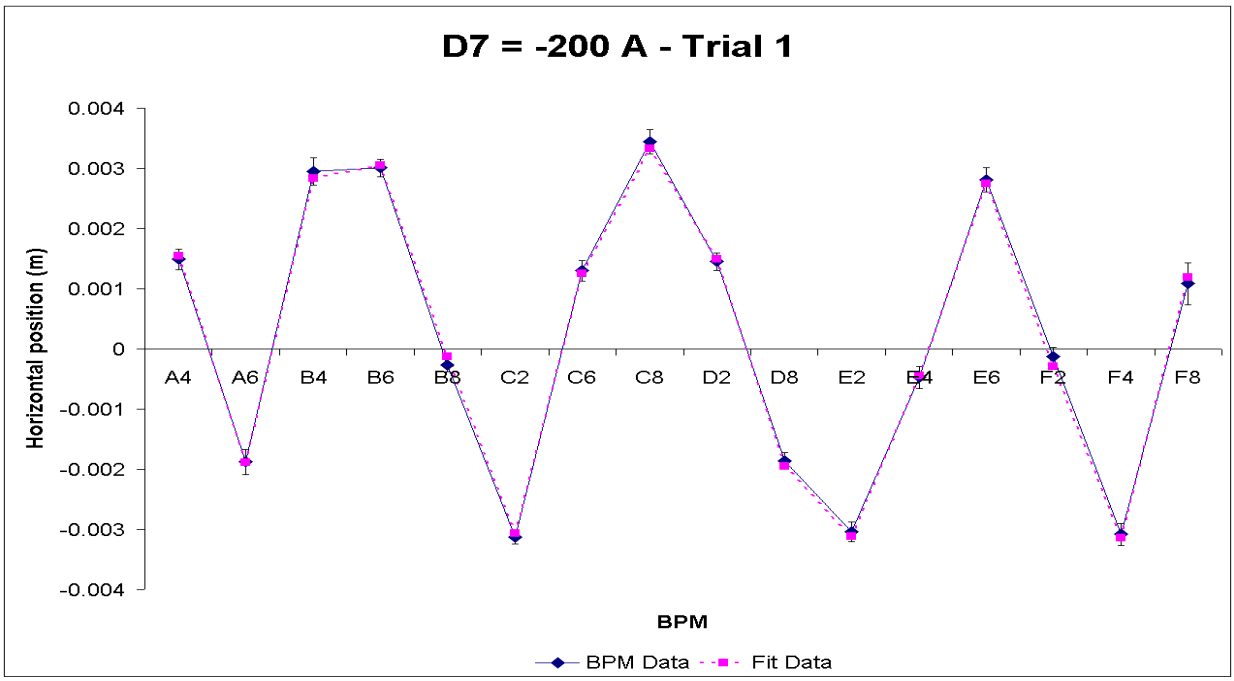

Figure 44

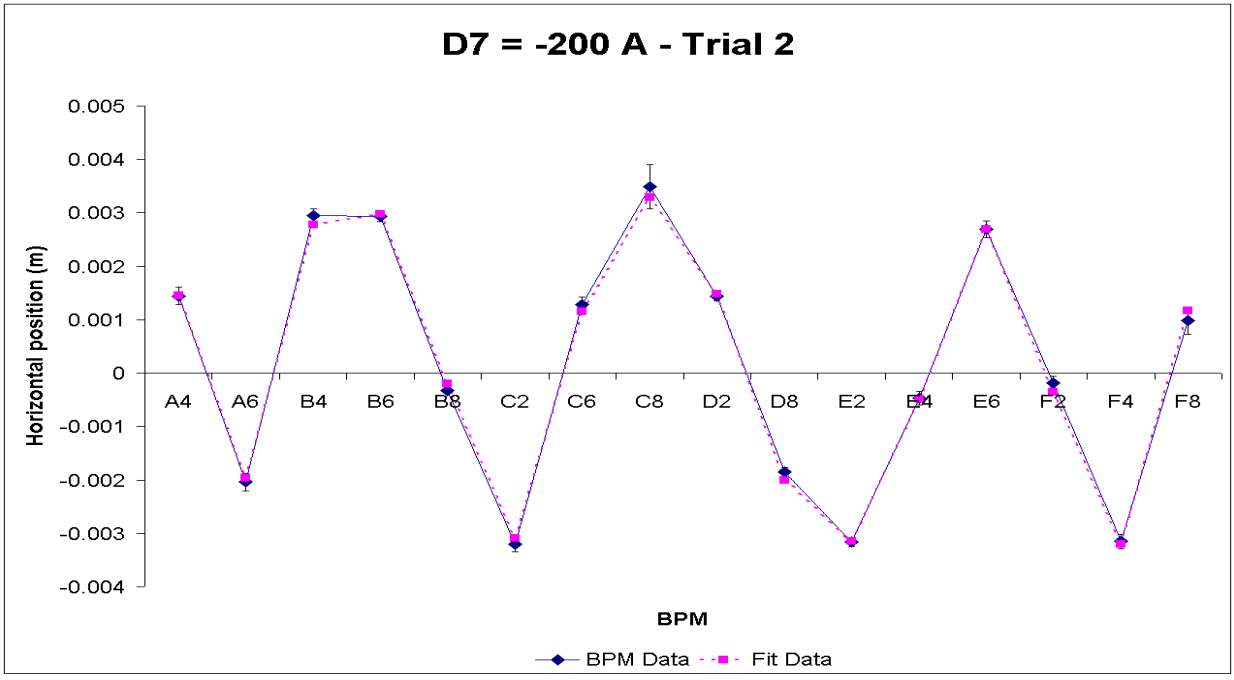

Figure 45

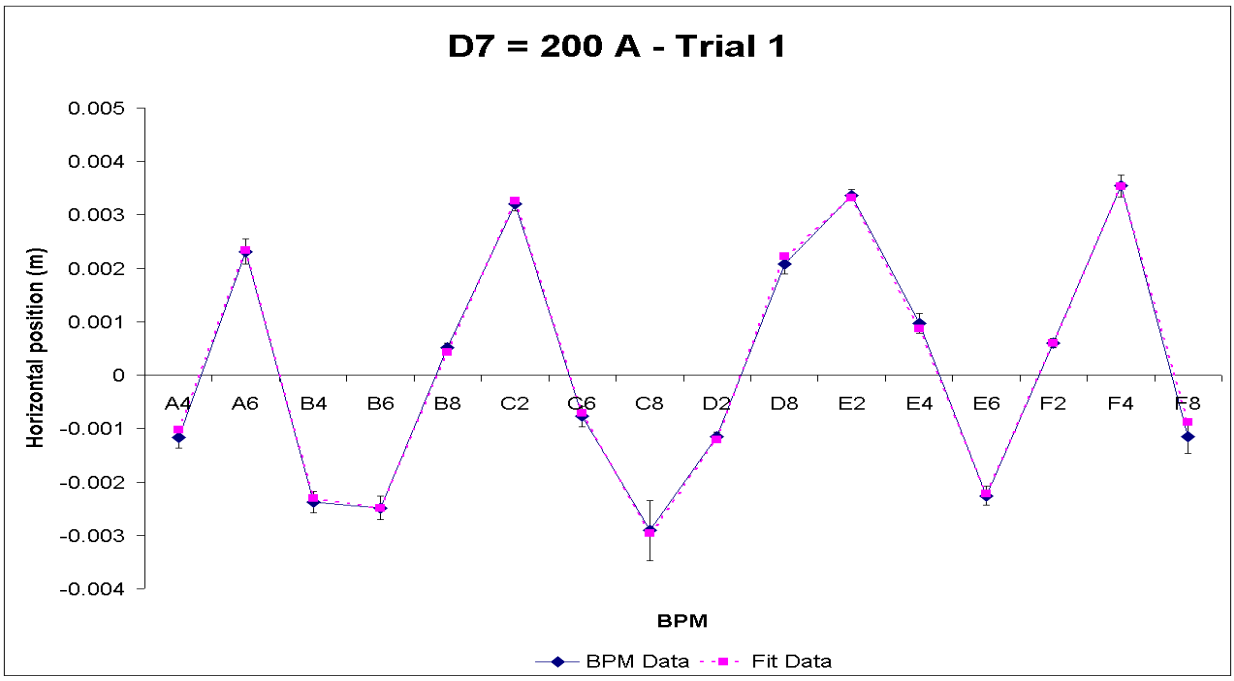

Figure 46

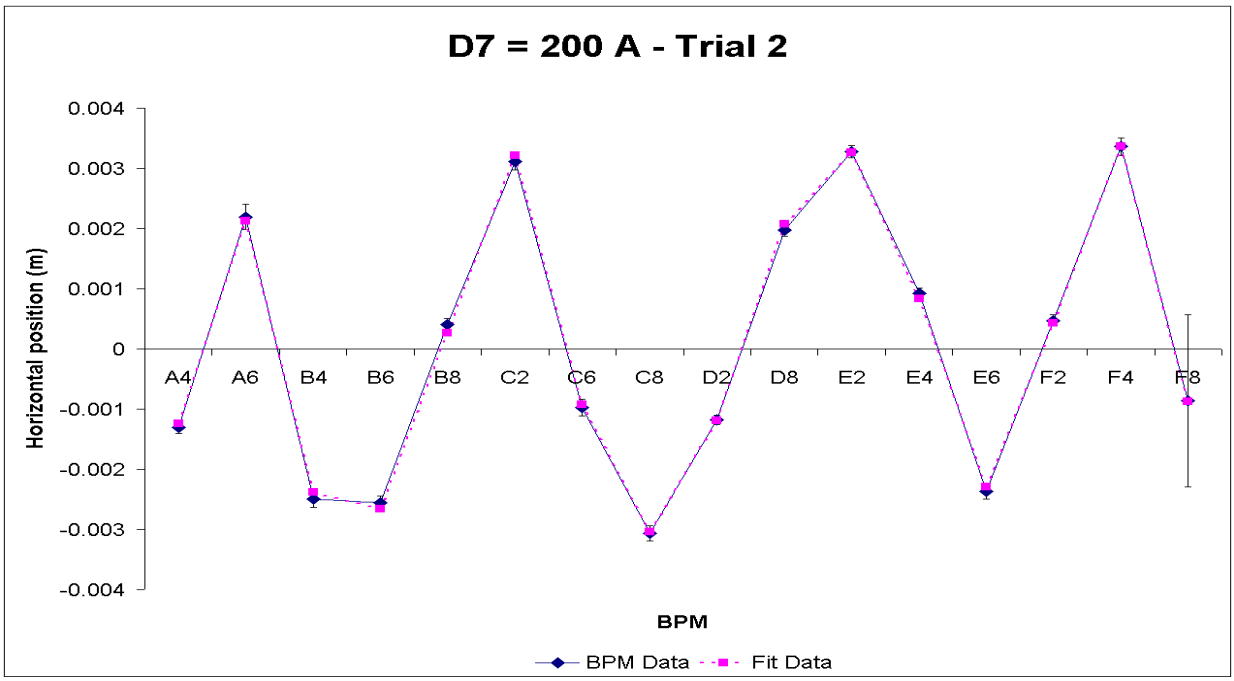

Figure 47

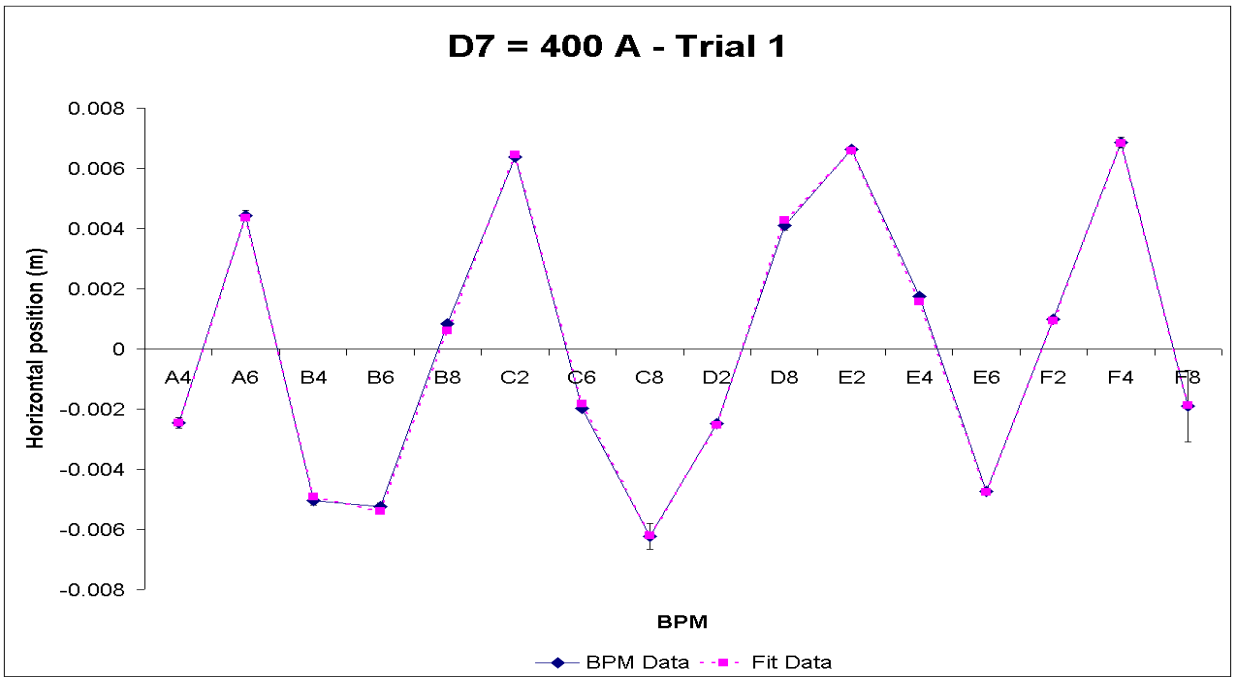

Figure 48

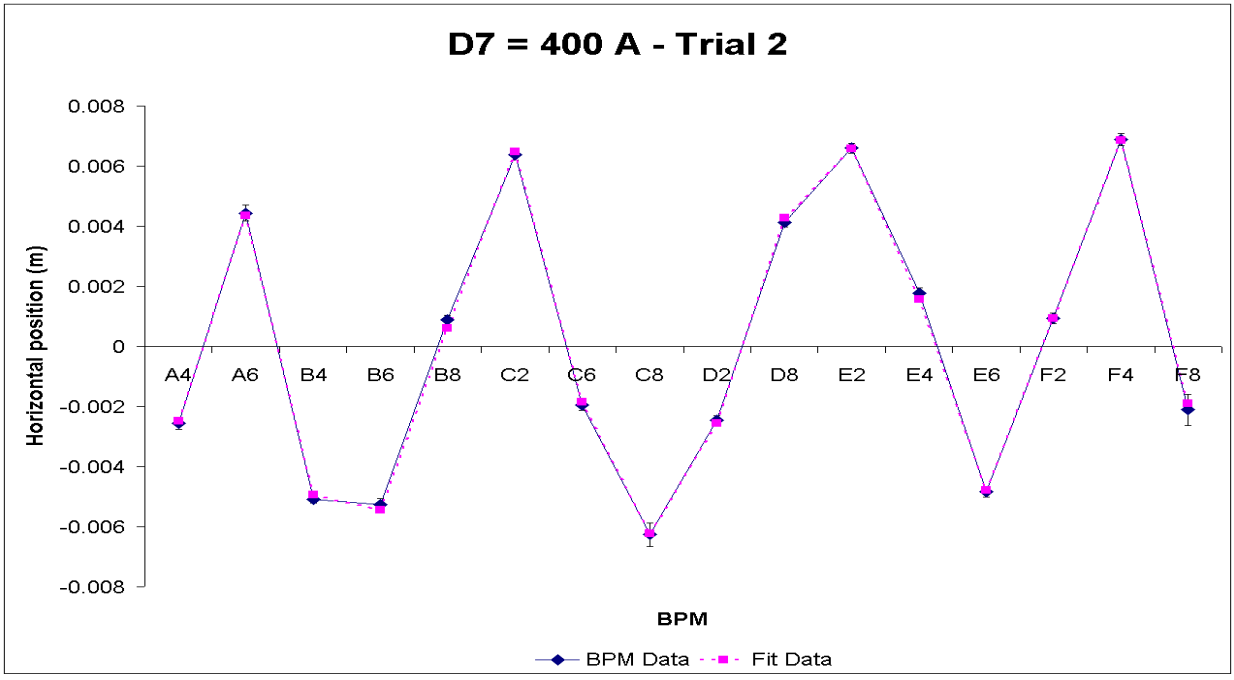

Figure 49

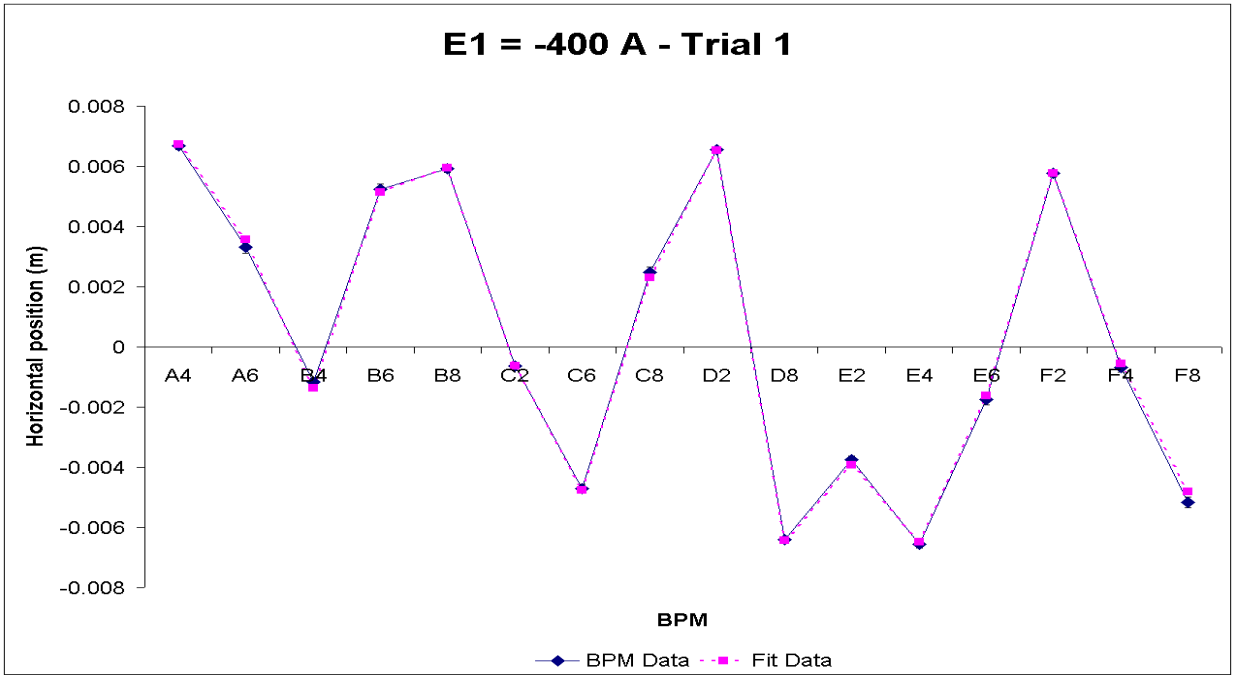

Figure 50

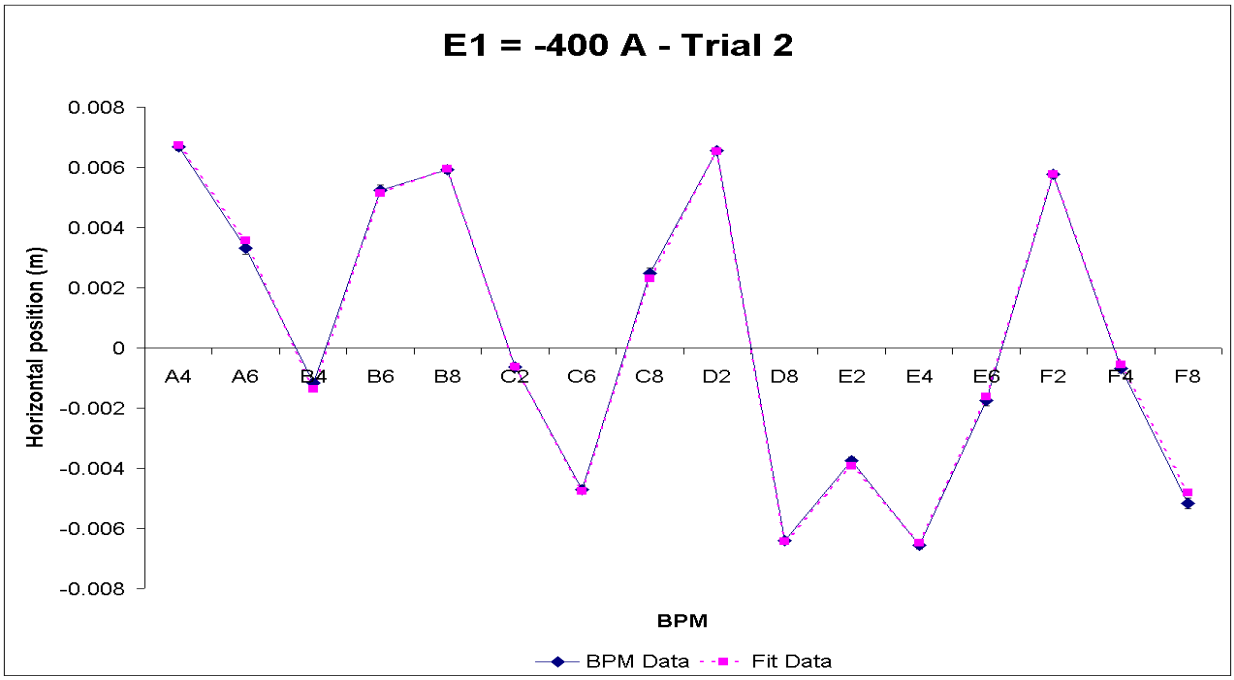

Figure 51

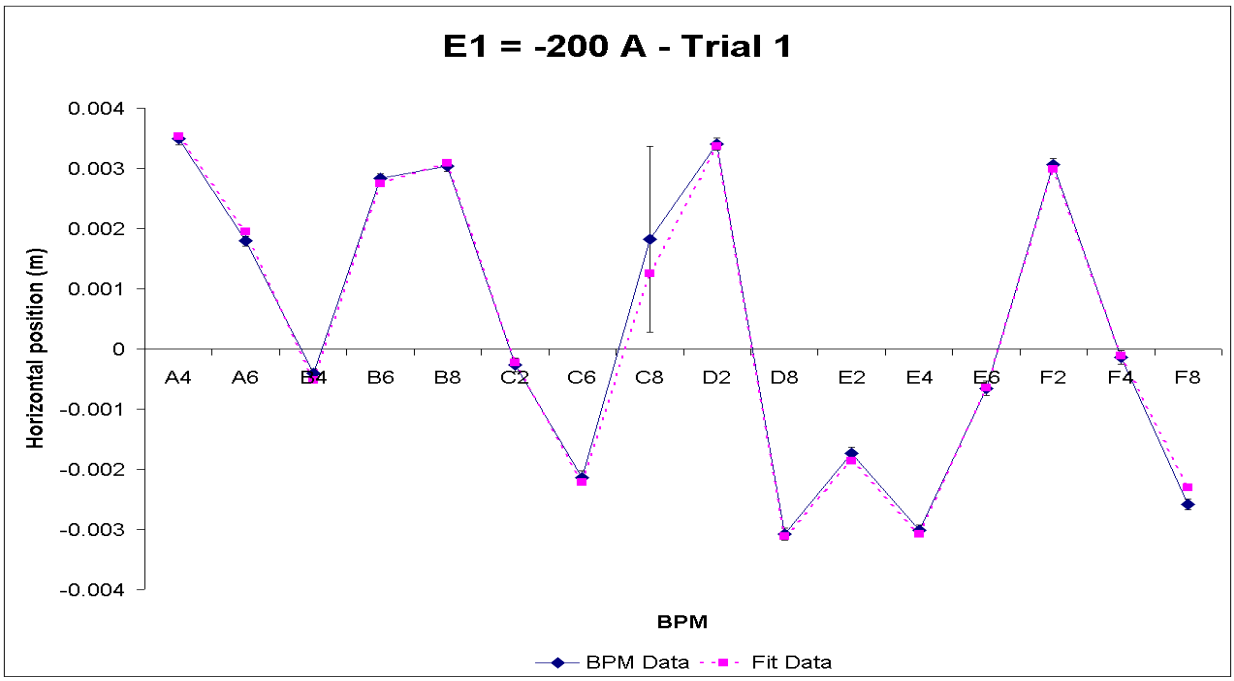

Figure 52

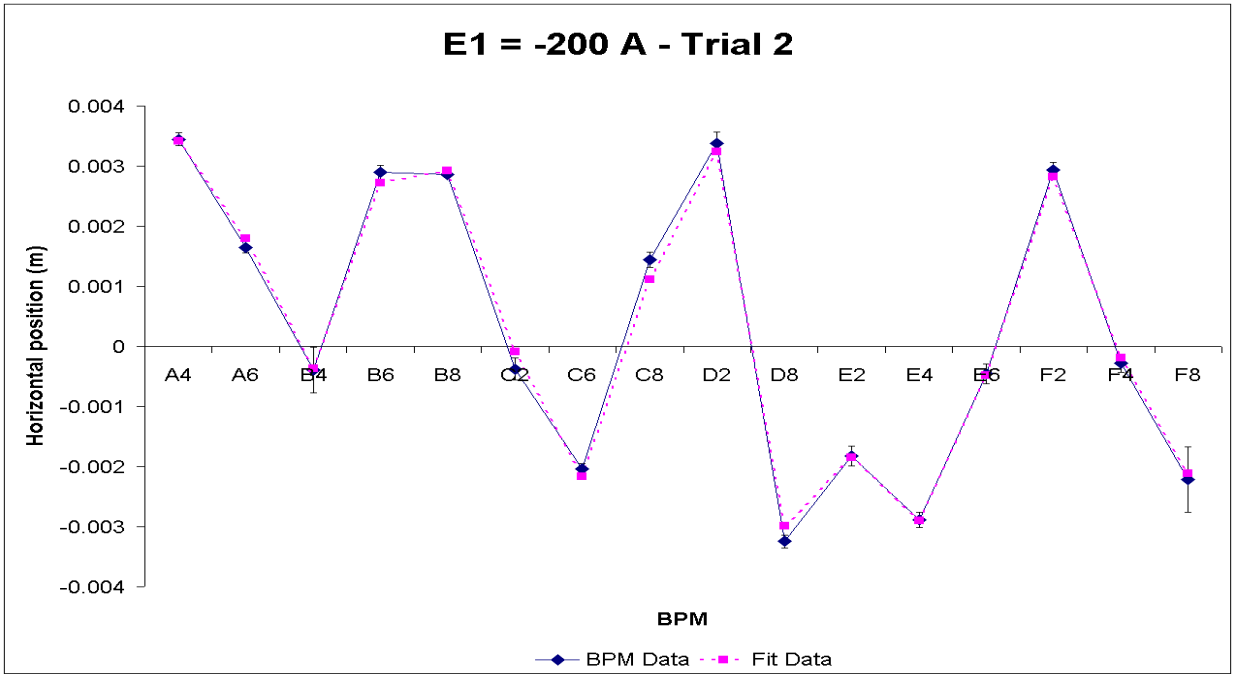

Figure 53

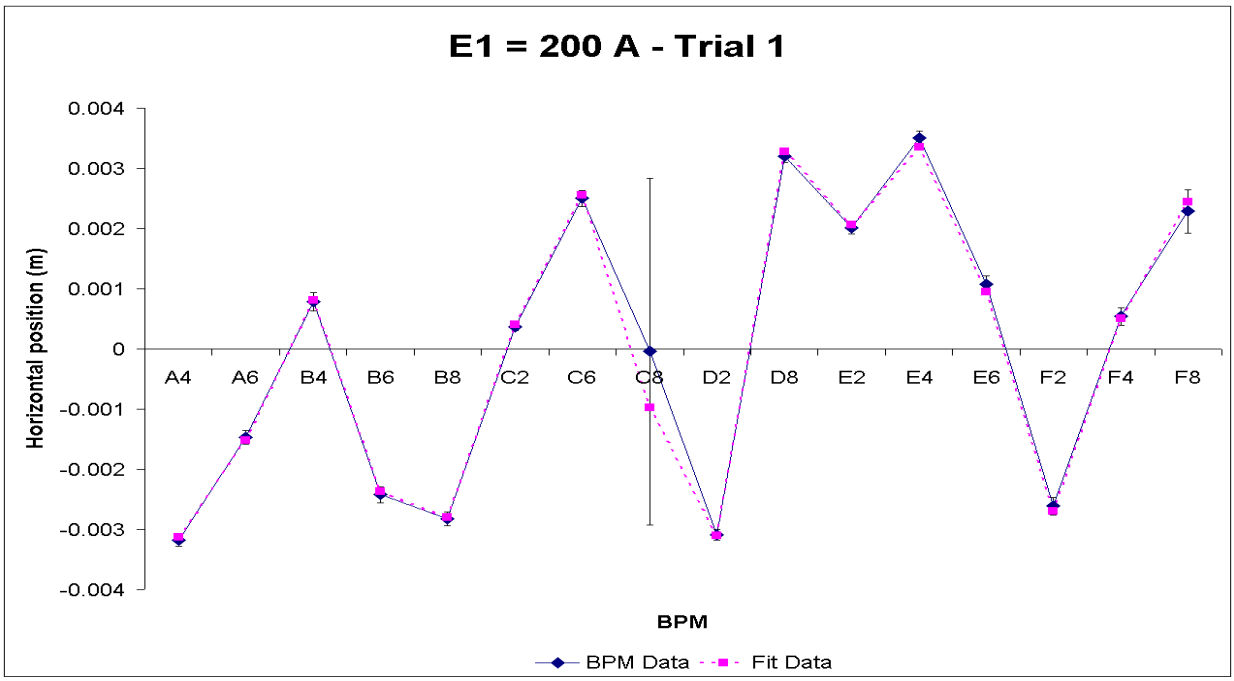

Figure 54

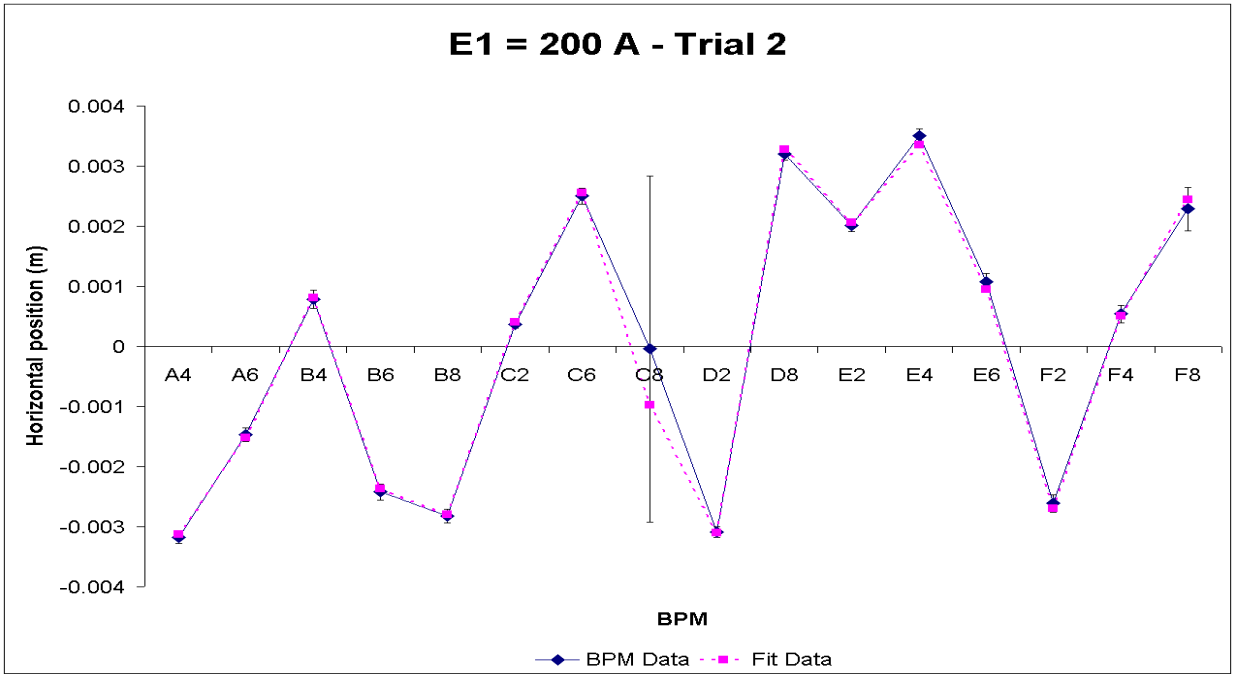

Figure 55

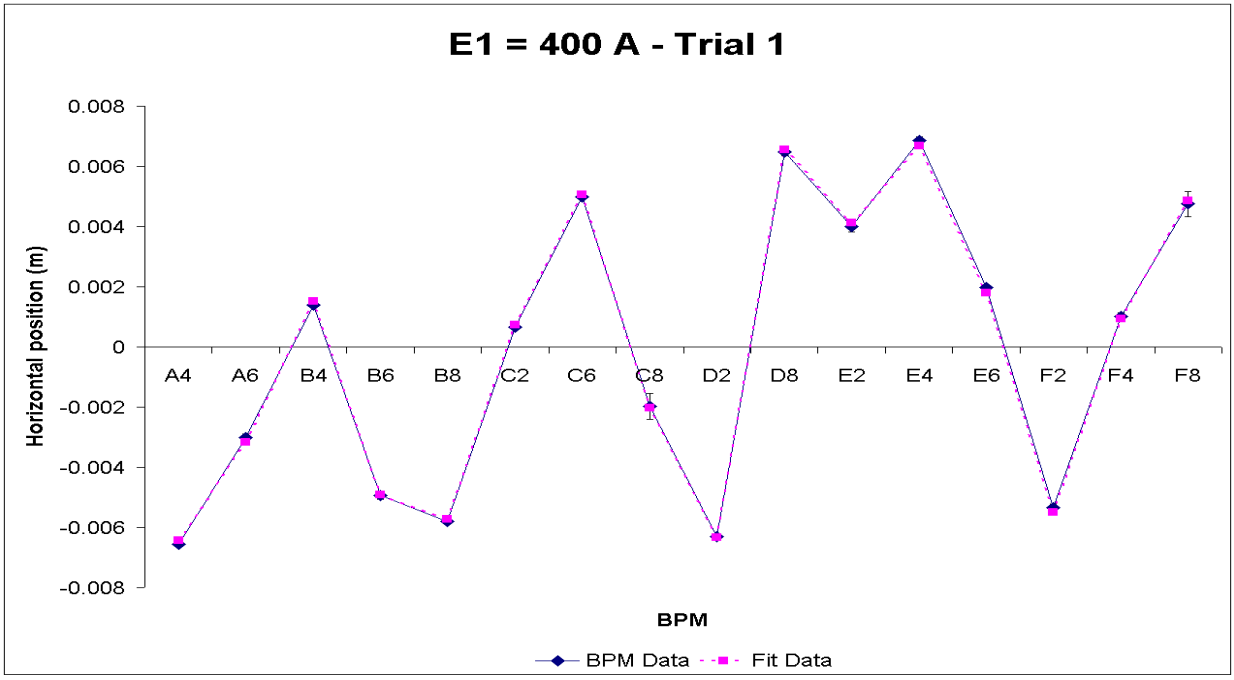

Figure 56

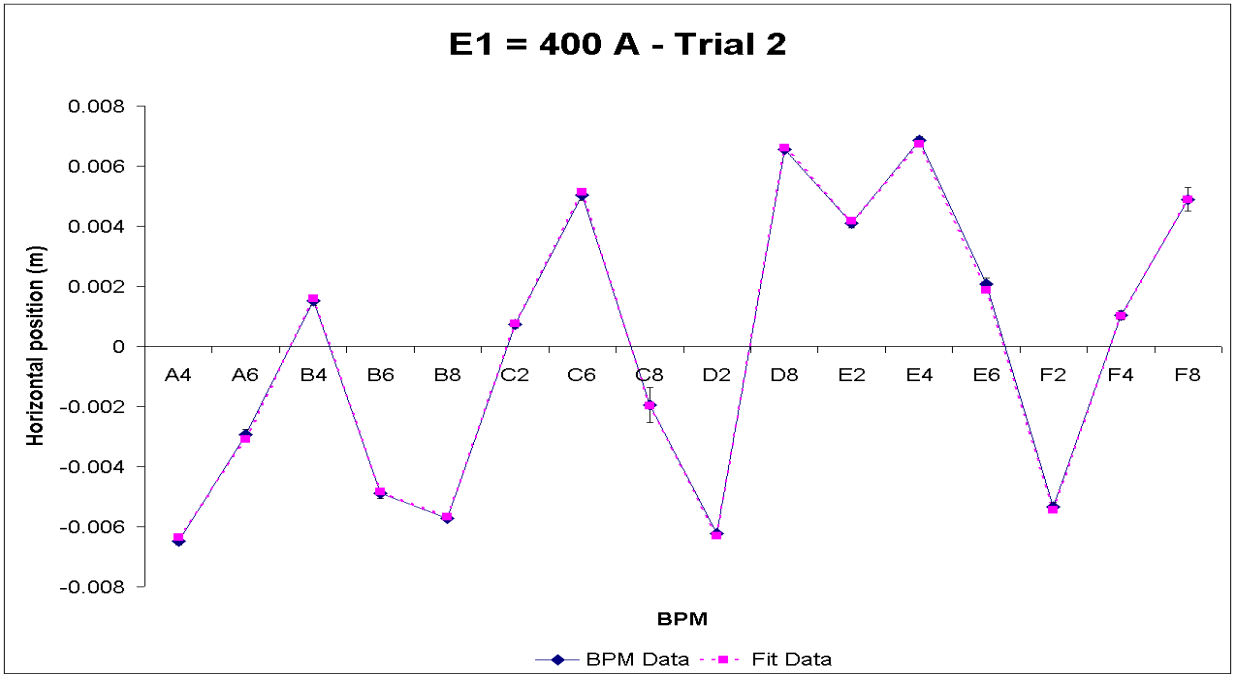

Figure 57

References

[1] Thern, R., *Booster Dipole Production Measurements*, Booster Technical Note 190, 1991.

[2] BNL MAD Booster Model.

[3] S. Savaterri (private communication)

[4] C. Gardner, *NSRL7 Schedule and Parameters*, available at: http://www.cadops.bnl.gov/AGS/Operations/GardnerNotes/NsrlRuns/Nsrl7.pdf, 2005.